Electronic Supplementary Material (ESI) for RSC Advances.
This journal is © The Royal Society of Chemistry 2021

Hybrid material by anchoring of ruthenium (II) imine complex to SiO_2: preparation, characterization and DFT studies

G. Eliad Benitez-Medina,*[a†] Raúl Flores,[b†] Luis Vargas,[a] Fernando Cuenú,[c] P. Sharma,[d] Miguel Castro*[b] and Alfonso Ramírez*[a]

a. Grupo de Investigación Catálisis, Universidad del Cauca, Calle 5 No. 4-70, Popayán, Colombia
b. Departamento de Física y Química Teórica, DEPg, Facultad de Química, Universidad Nacional Autónoma de México, C.P. 04510, Ciudad de México, México.
c. Grupo Química de Compuestos Organometálicos y Catálisis, Universidad del Quindío, Armenia, Colombia
d. Instituto de Química, Universidad Nacional Autónoma de México, Ciudad Universitaria, Circuito Exterior, Coyoacán 04510, Ciudad de México, México.

gerelid@hotmail.com

aramirez@unicauca.edu.co

miguel.castro.m@gmail.com

Supporting Information

Table of Contents

1 Spectra Data 4S

1.1 FT-IR Data 4S

1.2 Raman Spectroscopy 10S

1.3 XPS Spectroscopy 14S

1.4 Absorption Atomic Analysis 20S

1.5 Diffuse Reflectance Spectroscopy UV-Vis 21S

2 Thermogravimetric Analysis (TGA) 25S

3 Braunuer-Emmett-Teller (BET) and Barret-Joyner-Helenda (BHJ) analyses 26S

3.1 BET and BHJ analysis of **3a** solid 26S

3.2 BET and BHJ analysis of **3b** solid 31S

3.3 BET and BHJ analysis of **3c** solid 35S

3.4 BET and BHJ analysis of **3d** solid 38S

4 Theoretical Data 42S

4.1 Optimized structures 42S

4.1.1 XYZ coordinates 42S

4.2 IR Spectra 52S

4.3 TD-DFT UV-Vis Spectra 55S

4.3.1 Natural Transition Orbital 56S

4.3.2 $RuCl_2(P(Ph)_3)_2$(2-Py-CH)=N-CH_3 Natural Transition Orbitals Contour Plots 58S

4.3.4 $RuCl_2(P(OPh)_3)_2$(2-Py-CH)=N-CH_3 Natural Transition Orbitals Contour Plots 62S

1. Spectra Data

1.1 FT-IR Spectra

FT-IR spectra were recorded on a **Nicolet IR-200** with 32 scans and a resolution of 16 $cm^{-1}s^{-1}$, and the deconvolution process was recorded in the Fityk 0.9.8. Software (A curve fitting and data analysis program).

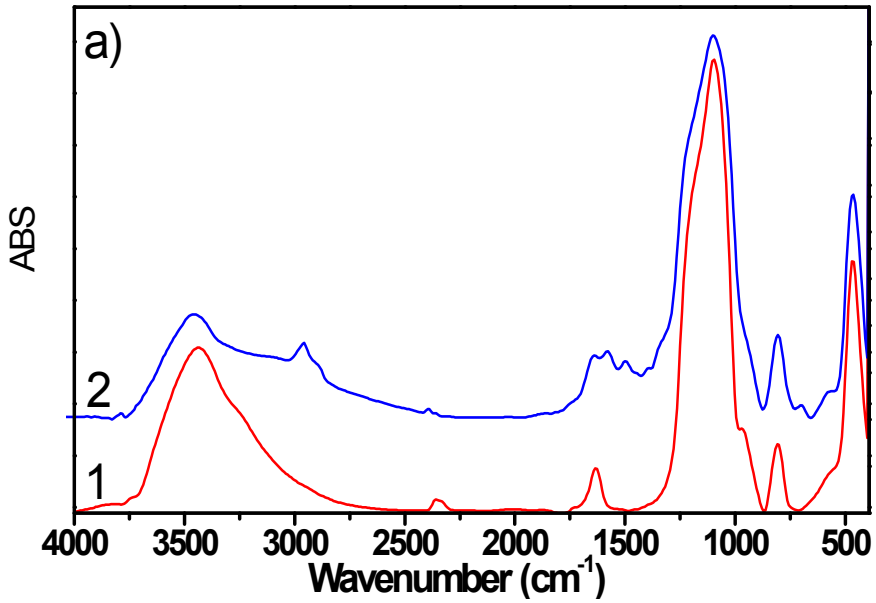

Figure S1. FT-IR spectra of the (1) Degussa silica, and (2) 3-Aminopropyltriethoxysilane functionalized Degussa silica (**1a)**.

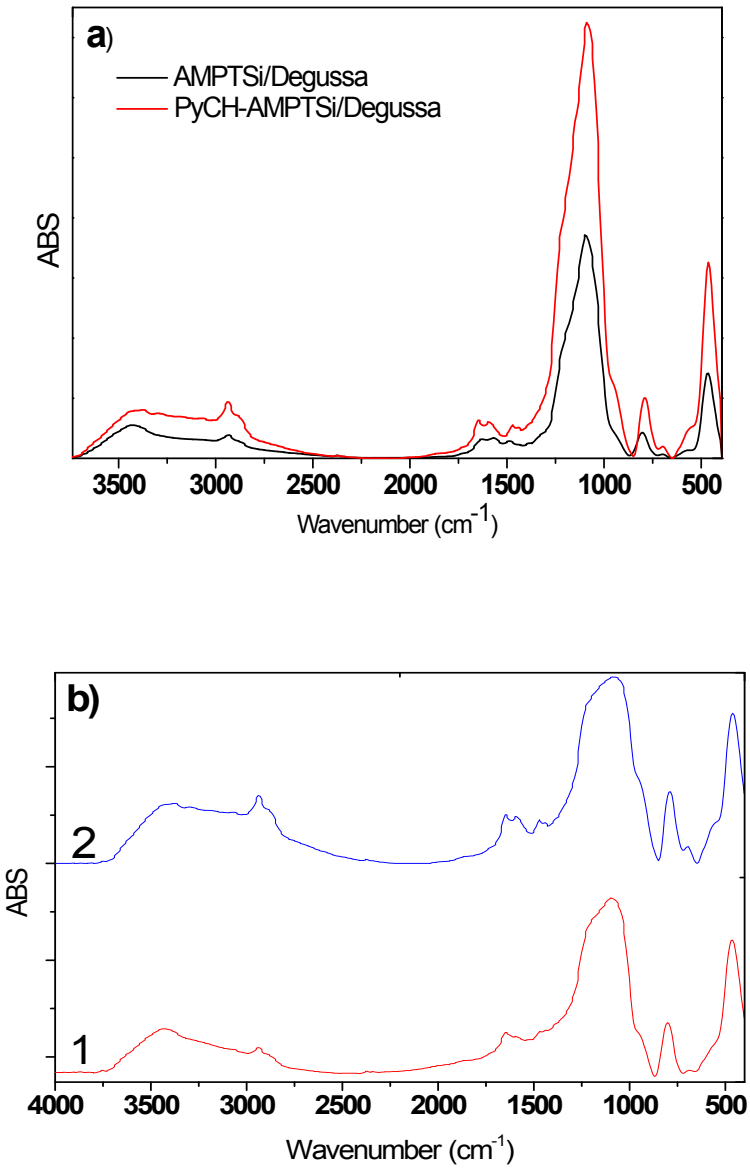

Figure S2. (a) FT-IR spectra of the (black line) AMPTSi/Degussa, (red line) activated AMPTSi/Degussa with 2-Pyridinecarboxaldehyde, **2-PyCH-AMPTSi/Degussa**. (b) FT-IR spectra of the (1) material **2a** and (2) material **2b**.

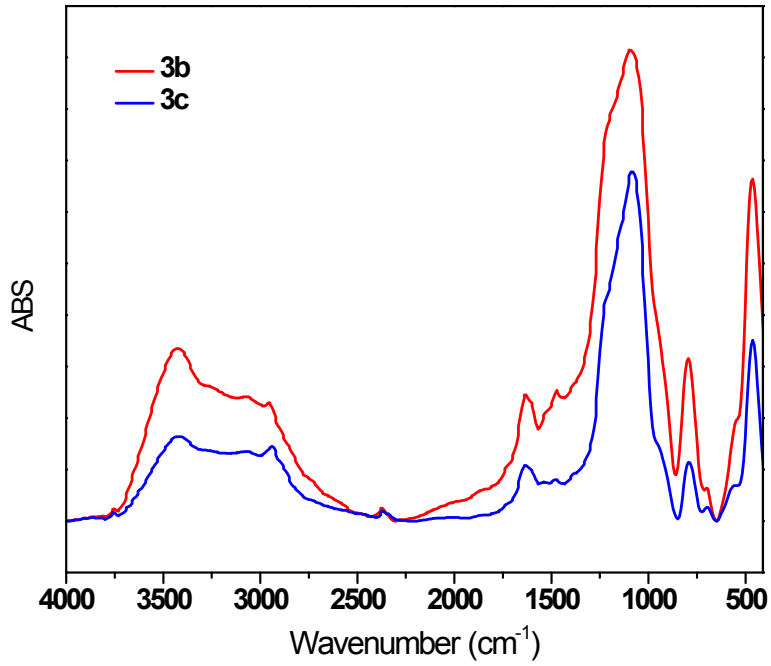

Figure S3. FT-IR Spectra of the solids **$RuCl_2(P(OPh)_3)_2$-(2-PyCH)-AMPTSi/Degussa** (**3b**) and **$RuCl_2(P(OPh)_3)$2-(2-PyCH)-AMPTSi/MCM-41** (**3c**), in the region 4000-500 cm^{-1}.

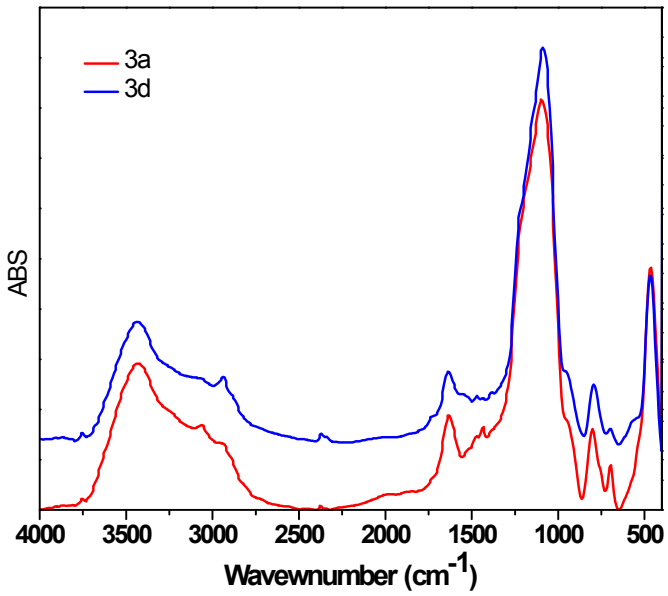

Figure S4. FT-IR Spectra of the solids **$RuCl_2(PPh_3)_2$-(2-PyCH)-AMPTSi/Degussa** (**3a**) and **$RuCl_2(PPh_3)$2-(2-PyCH)-AMPTSi/MCM-41** (**3d**).

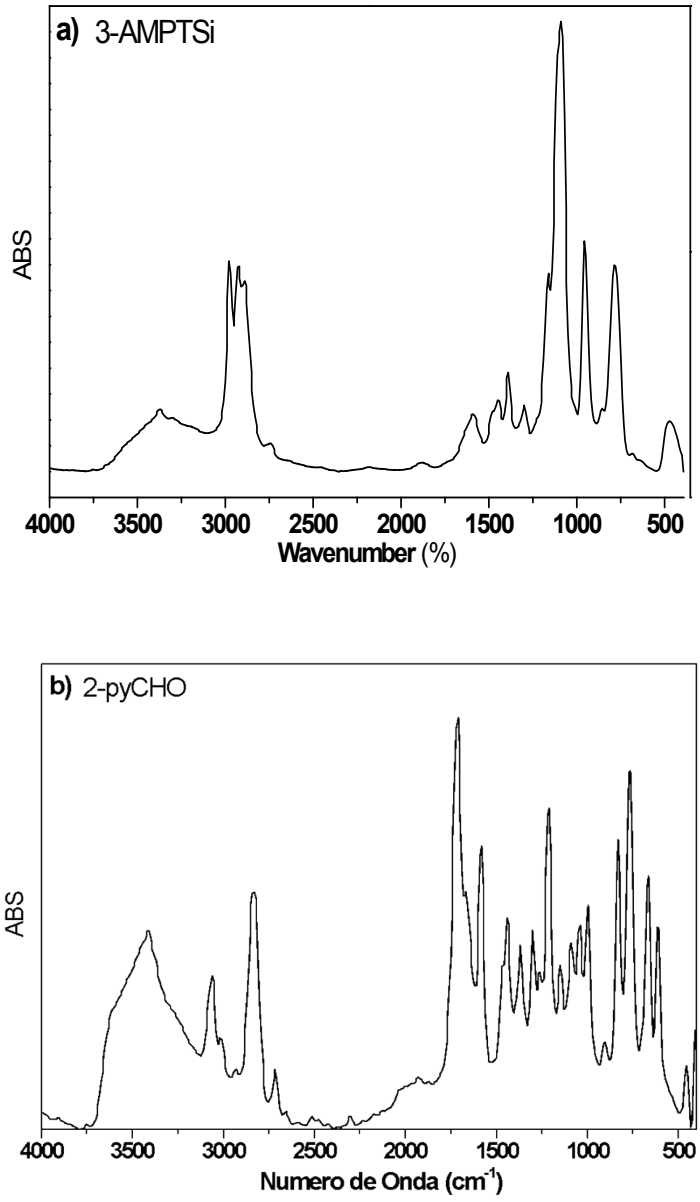

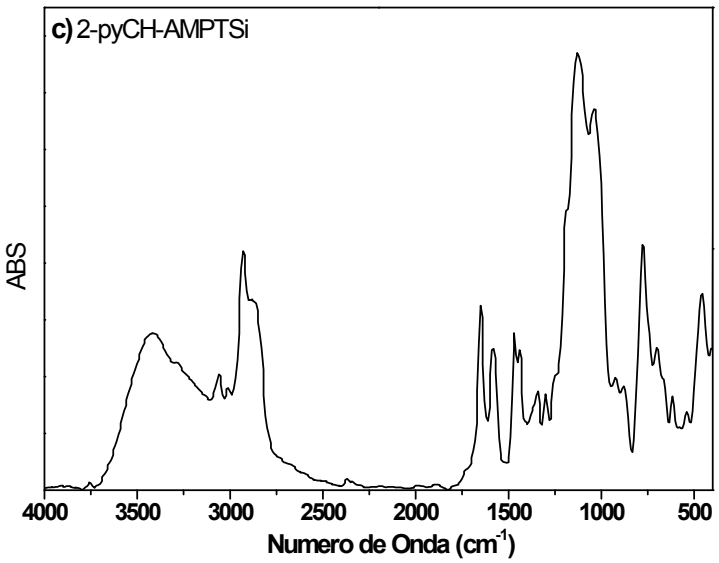

Figure S5. FT-IR Spectra of the (a) 2-PyCHO and (b) 3-AMPTSi and (c) FT-IR spectrum of the reaction product 2-pyCH-AMPTSi.

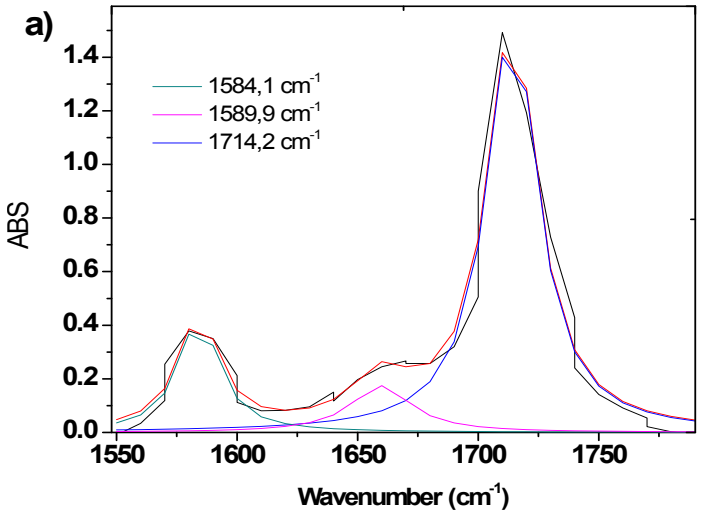

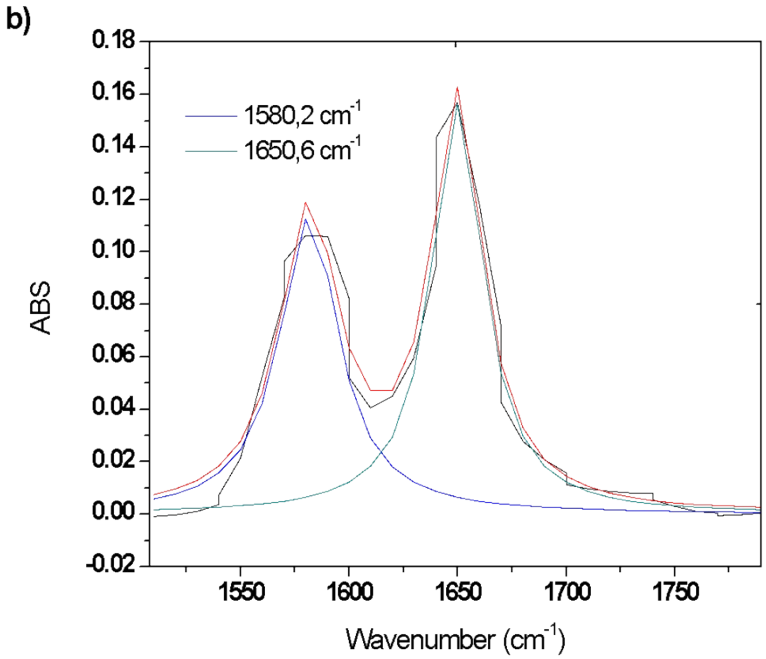

Figure S6. (a) Deconvolution in the FT-IR spectrum of the 2-PyCHO (b) Deconvolution in the FT-IR spectrum of the 2-PyCH-AMPTSi.

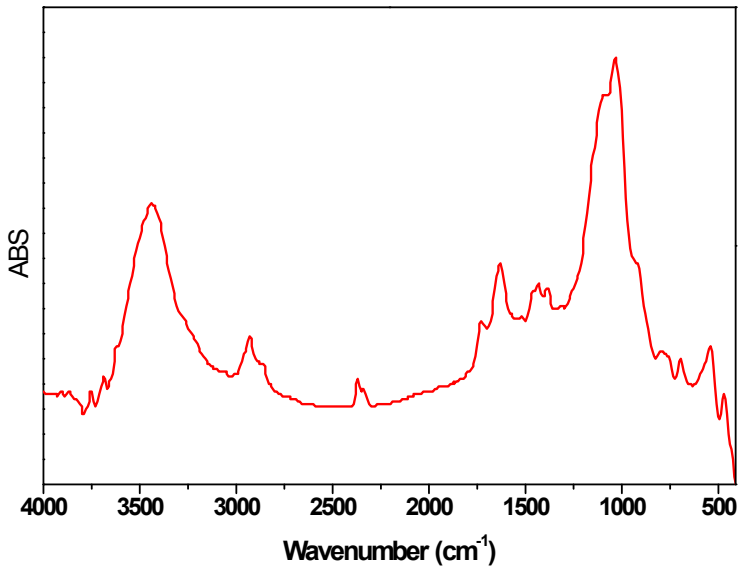

Figure S7. FT-IR spectrum of the $[RuCl_2(PPh_3)_2(2pyCH\text{-}AMPTSi)]$ **3e**

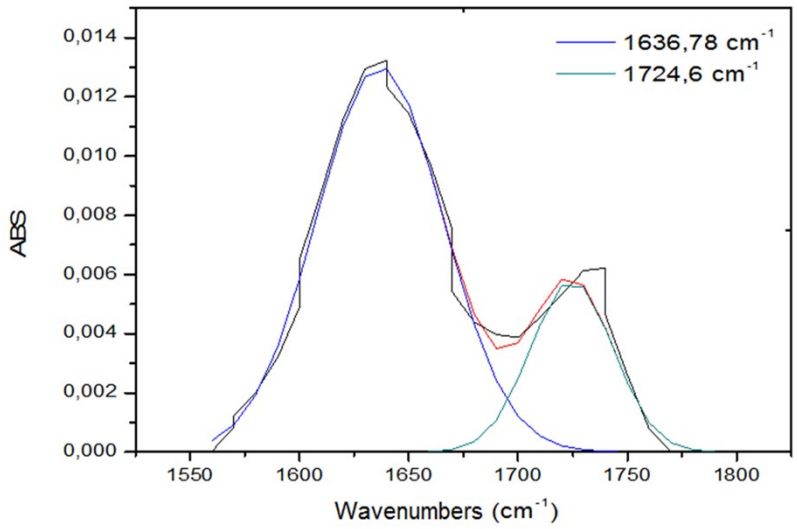

Figure S8. Deconvolution between 1550 and 1780 cm^{-1} in the FT-IR spectrum of the **3e**.

1.2 Raman Spectroscopy

The RAMAN spectra were obtained using a **Raman Perkin Elmer NIR FT-Raman SpectRUm GX** spectrophotometer, and the deconvolution process was recorded in the Fityk 0.9.8. Software (A curve fitting and data analysis program).

A small amount of sample (a few milligrams) was deposited on a glass slide. The analyzes were carried out according to the operating conditions determined (Table S1)

Table S1. Operating conditions on RAMAN spectroscopy.

	Laser (nm)	Filter	Hole (µm)	red (g/mm)	Objective	Scan range (cm-1)	Exposition time (s)	Number of acquisitions	Mode of acquisition	Spike filter
3a 3b 3c 3d	514,5	D1	200	600	X100	50-2000	200	5	Multiple windows	Multi (auto add)

Table S2. Frequencies of observed bands in **3a**-**3d** solids.

Sample	Frequencies of observed bands (cm^{-1})									
3a	60,0	76,1	101,3			346,8	460,5	480,8	533,9	
3b	58,4	77,3	110,5		211,5	351,7	450,6	480,5	555,4	
3c	58,1	77,7	112,9	145,6	205,6	349,8	434,5	489,4		621,0
3d	60,3	78,7	105,7	155,9	192,2	344,2	439,5	491,6		624,0

3a	658,8	695,0		803,5	929,8	957,3	1003,2	1031,6	1052,4	1105,1
3b	660,7	700,3		810,6		943,5	990,5	1034,8	1060,5	1093,9
3c	661,5	691,4	719,6	802,6		947,4		1036,4	1059,5	1108,6

3d	661,5	694,4	722,7	806,4		953,9	1003,9	1036,8	1060,7	1103,2

3a	1124,7	1160,5	1187,9	1243,3	1298,6	1343,4	1388,2	1450,7	**1472,8**	**1548,6**
3b		1166,4		1249,5	1293,8	1320,7		1446,7	**1471,4**	**1553,7**
3c		1161,7		1254,4	1296,9	1337,5	1392,2	1454,1	**1474,5**	**1551,7**
3d		1164,9		1253,0	1299,8	1332,7	1398,1	1457,4	**1474,6**	**1555,4**

3a	**1607,0**	1648,5	
3b	**1606,7**		1795,9
3c	**1606,3**		
3d	**1604,8**	1651,9	

The Raman spectra of the four samples present many common bands. Raman spectra of samples **3c** and **3d** are very similar, only two additional bands appear on the spectrum of the **3c** sample, at 1003,9cm^{-1} and 1651,9cm^{-1}. The bands at 1470cm^{-1}, 1550cm^{-1} and 1600cm^{-1} correspond to the vibrations of the C=C bonds of the complex.[1-2] the band at 1030cm^{-1} can be attributed to the deformation of the group =C-H in the plane and the band at 1100cm^{-1} to the vibration of the P-Ph bond. The band at 800cm^{-1} can correspond to the deformation vibration in the pyridine ring.[1]

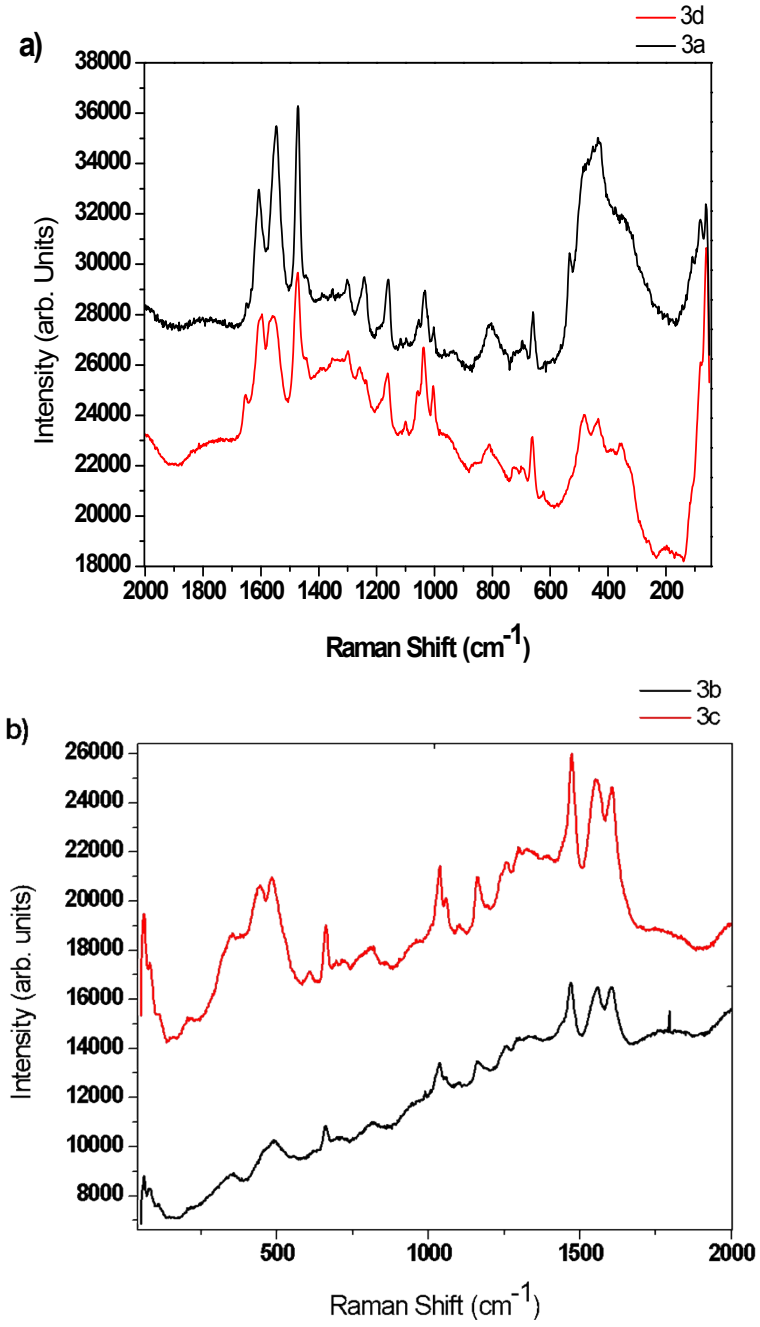

Figure S9. RAMAN spectra of the solids **3a**-**3d**; (a) **3a** (black line) and **3d** (red line), (b) **3b** (black line) and **3c** (red line).

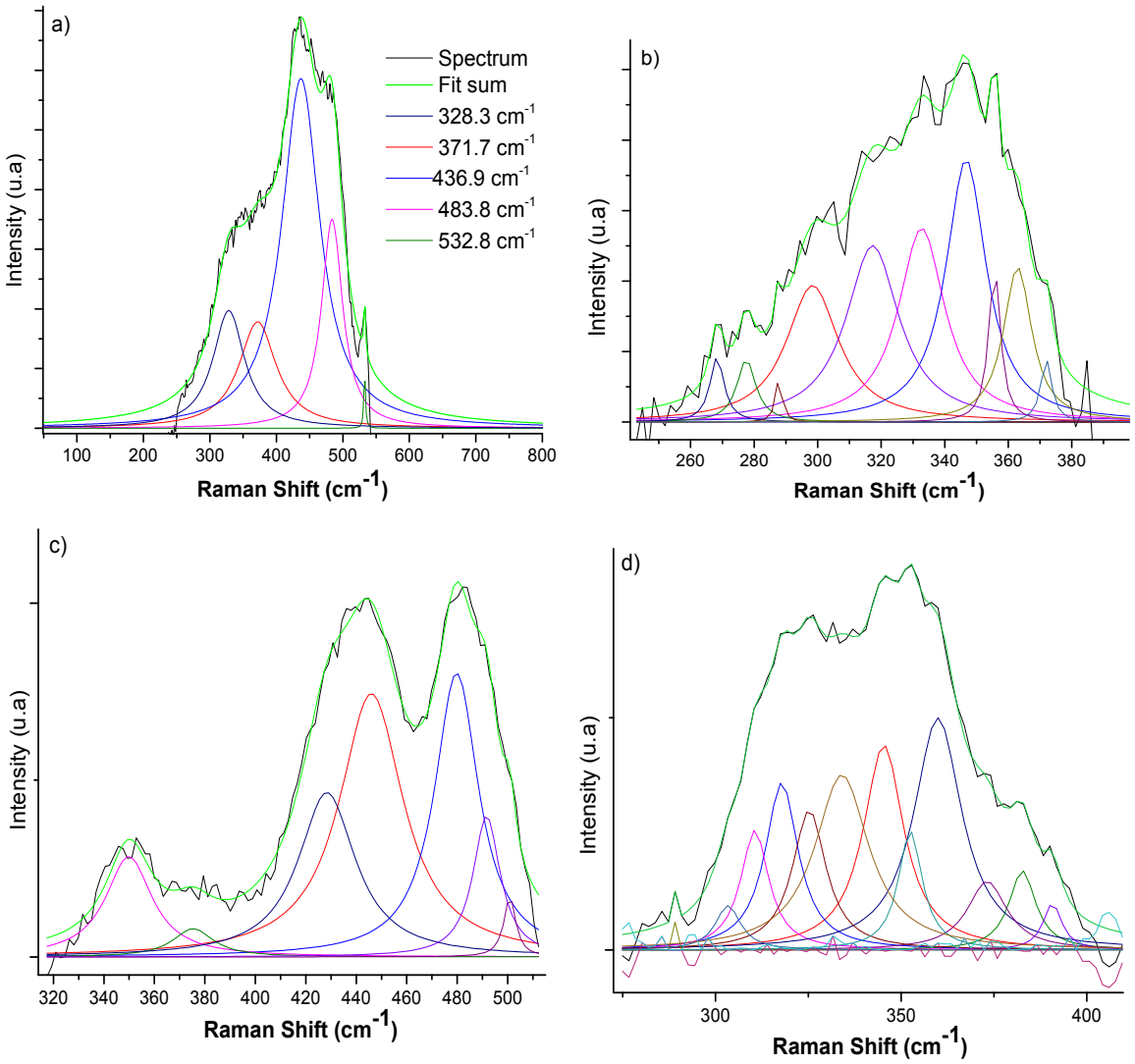

Figure S10. RAMAN spectra deconvolution plot of the solids **3a**-**3d**; (a) **3a**, (b) **3d**, (c) **3b** and (d) **3c**.

(1) G. Socrates, Infrared and Raman characteristic group frequencies, *Wiley*, London, 2008

(2) T. E. Chavez-Gil, D.L.A. de Faria, H. E. Toma, *Vibrational Spectroscopy*, 16 (1998) 89-92

1.3 XPS spectroscopy

XPS analyses were performed using **VG S-Probe XPS spectrometer** monochromatic, with a monochromatic aluminum AlKα(1486.6 eV) anode X-ray source, 45° takeoff angle (q=45°), the voltage and power of the source was 10KV and 200 W respectively

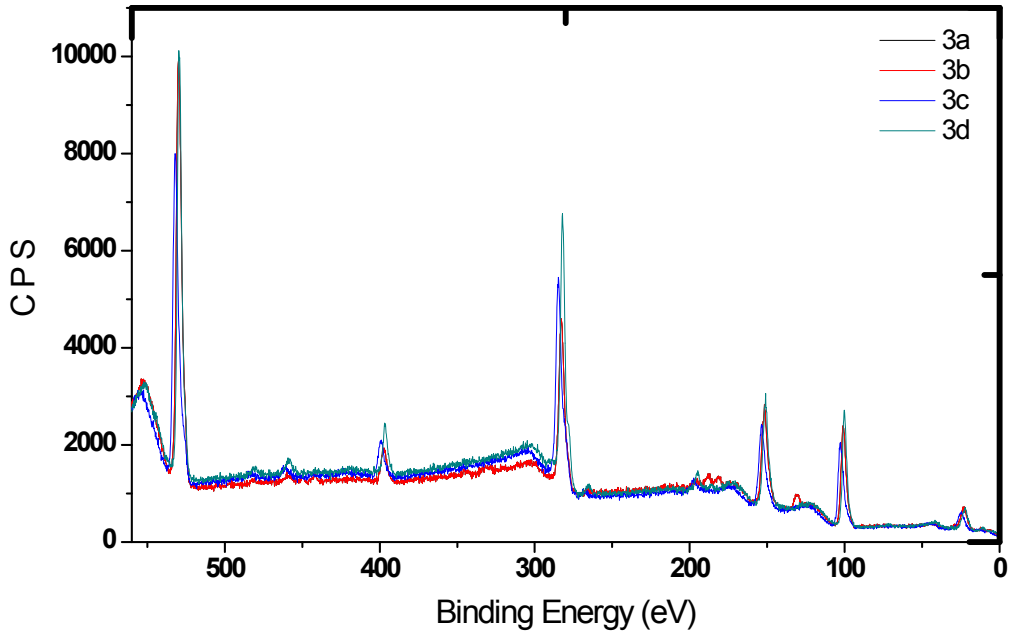

Figure S11. XPS Spectra of the **3a**-**3d** solids

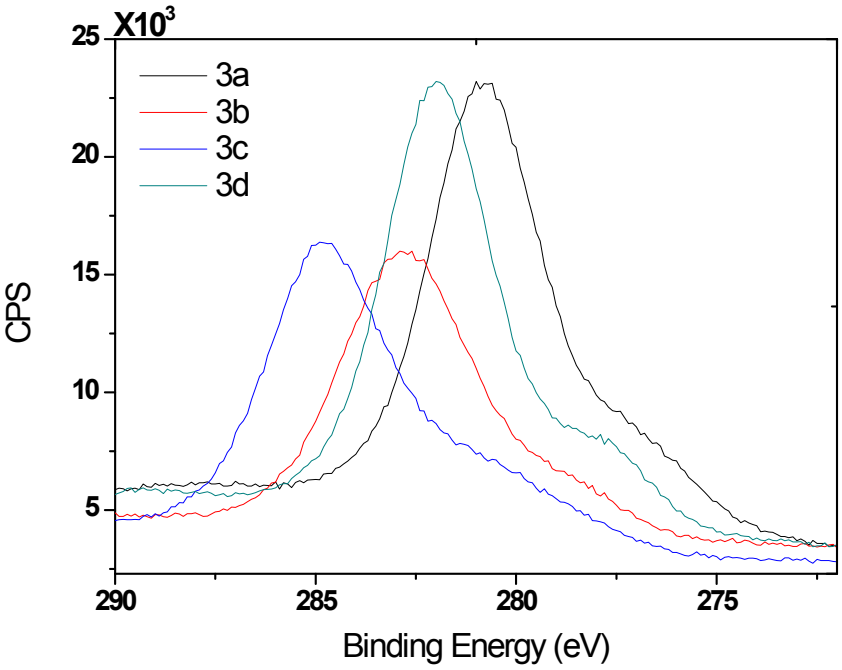

Figure S12. XPS Spectra of the **3a**-**3d** solids in the region corresponding to the Binding Energies (BE) **C1s, Ru 3d$_{5/2}$** y **Ru 3d$_{3/2}$.**

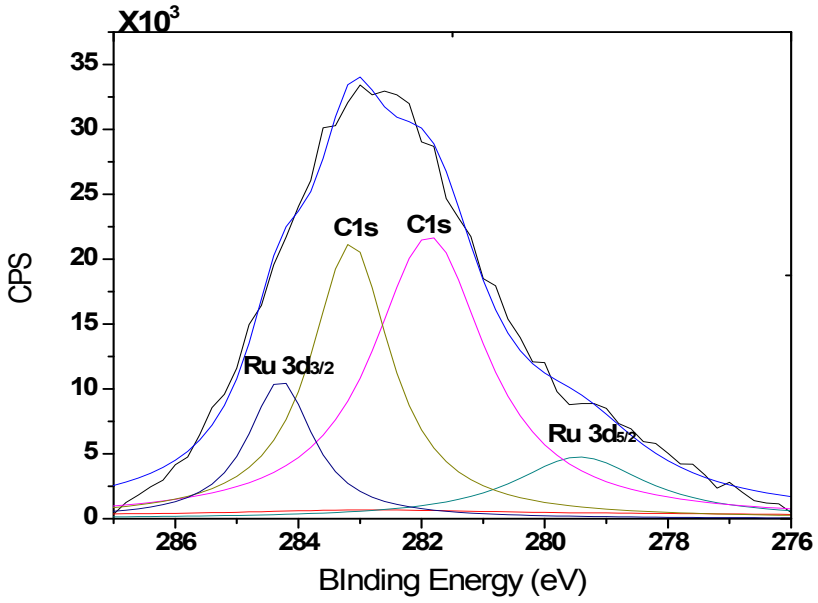

Figure S13. Deconvolution in the XPS Spectrum of the **3b** solid in the region corresponding to the Binding Energies (BE) **Ru 3d$_{3/2}$, Ru 3d$_{6/2}$ and C 1s**.

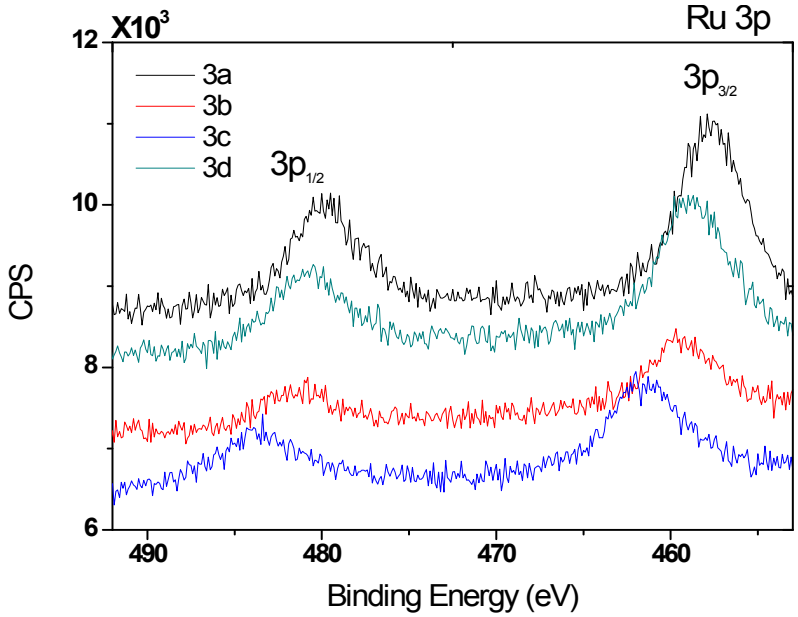

Figure S14. XPS Spectra of the **3a**-**3d** solids in the region corresponding to the Binding Energies (BE) **Ru 3p$_{3/2}$** and **Ru 3p$_{1/2}$**.

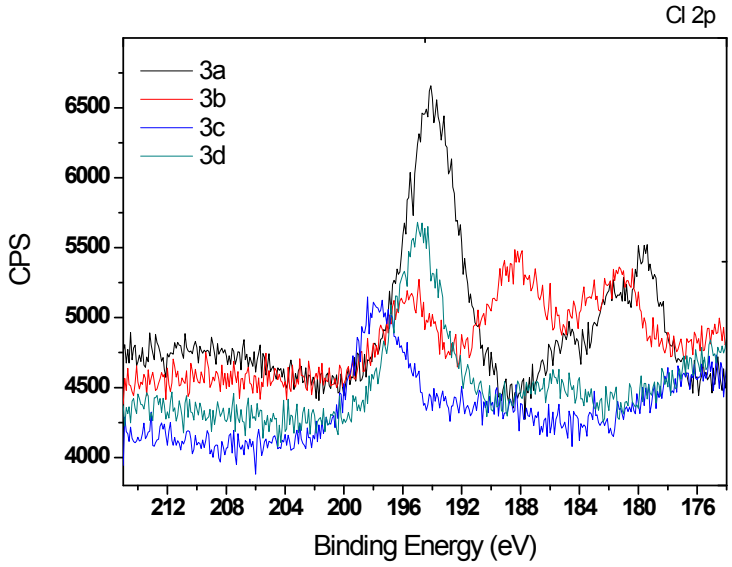

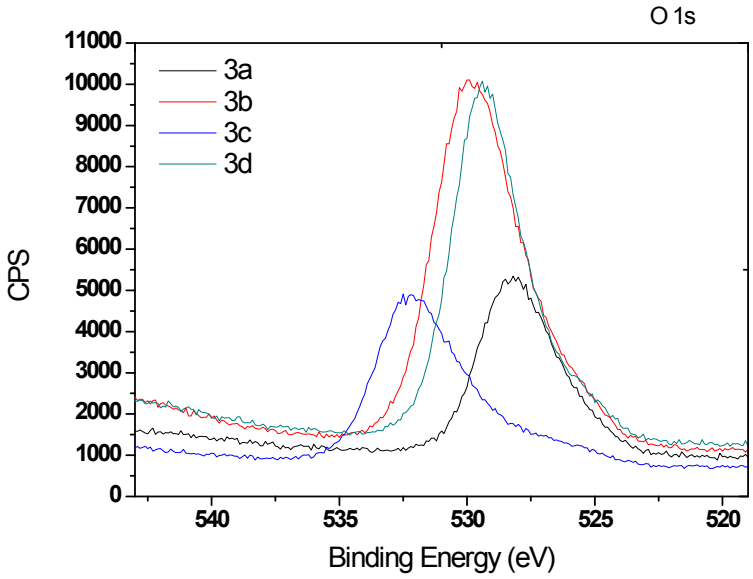

Figure S15. XPS Spectra **3a**-**3d** solids in the region corresponding to the Binding Energies (BE) **Cl 2p** and **O 1s**.

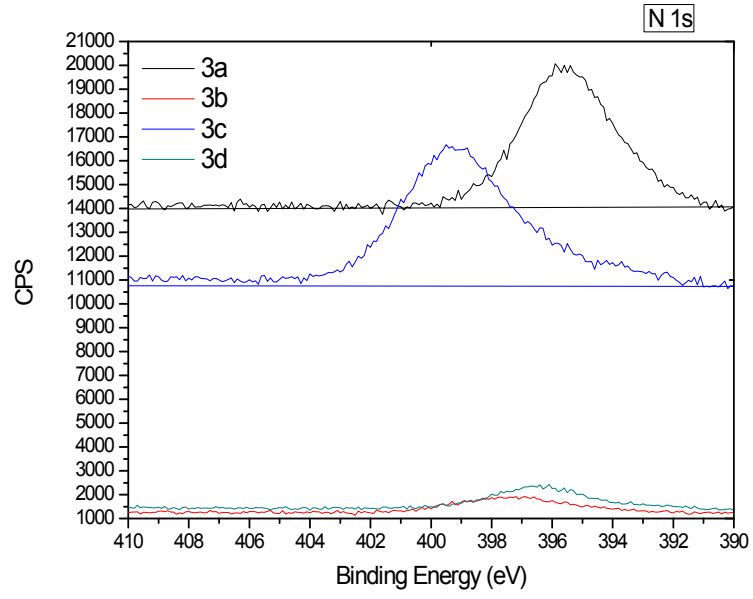

Figure S16. XPS Spectra **3a**-**3d** solids in the region corresponding to the Binding Energy (BE) **N 1s**.

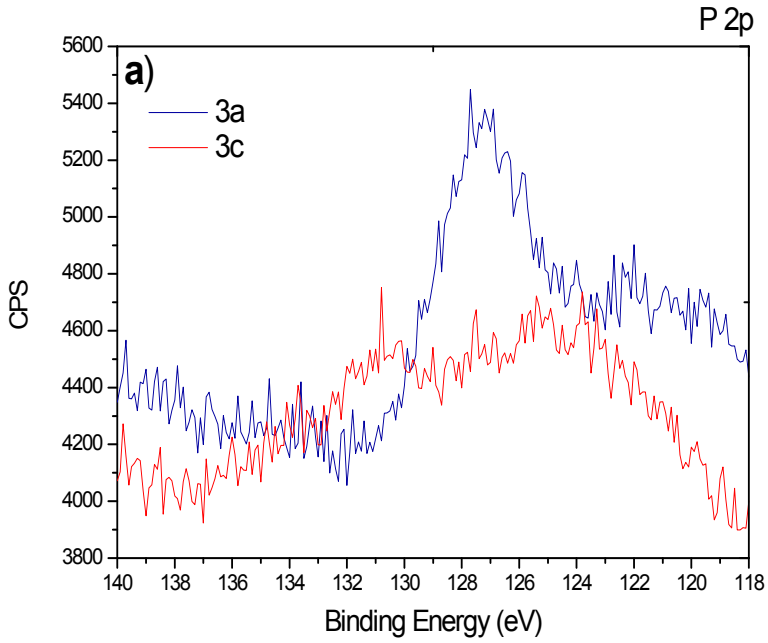
P 2p
a)
3a
3c
CPS
Binding Energy (eV)

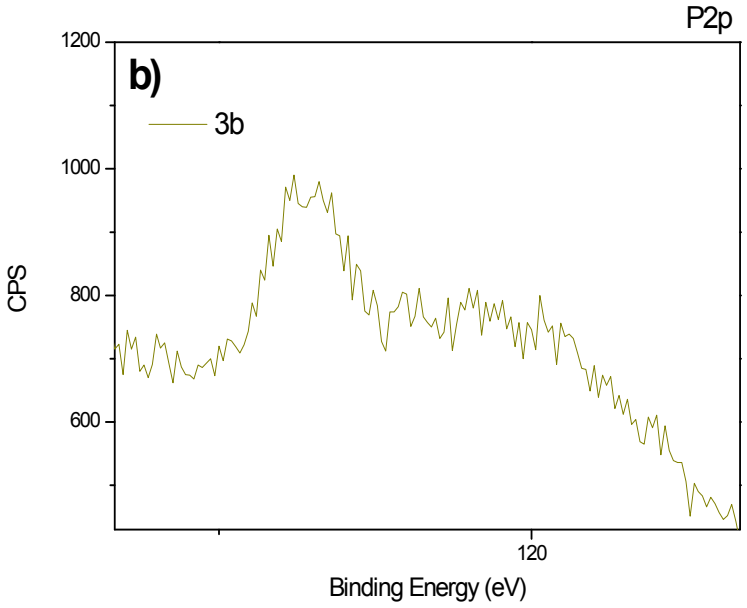
P2p
b)
3b
CPS
Binding Energy (eV)

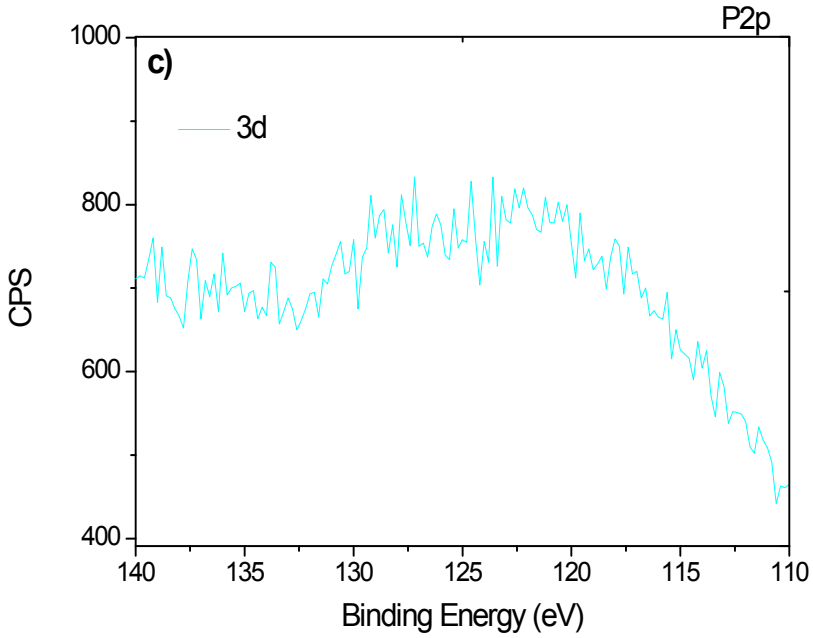

Figure S17. XPS Spectra of the **3a**-**3d** solids in the region corresponding to the Binding Energy (BE) **P2p**; (a) XPS spectra of the **3a** and **3c** solids, (b) XPS spectrum of the **3b** solid, and (c) XPS spectrum of the **3d** solid.

1.4 Atomic Absorption Analysis

Ruthenium is determined by Atomic Absorption to perform the assay; it is necessary to mineralize the sample.

The sample is weighed and then dissolved in 5 ml of hydrochloric acid, 3 ml of nitric acid and 2 ml of hydrofluoric acid. Mineralization takes place for 1 hour at 1000W. Add 12 ml of boric acid to complex the excess hydrofluoric acid. Complexation takes place for 1 / 2H at 1000W.

Atomic Absorption Assay:

1) Ruthenium:

The wavelength used is 349.89 nm. The linearity range of standard solutions is 10 mg / L. Three standard solutions are prepared from certified solutions: 2 mg / L, 4 mg / L and 8 mg / L.

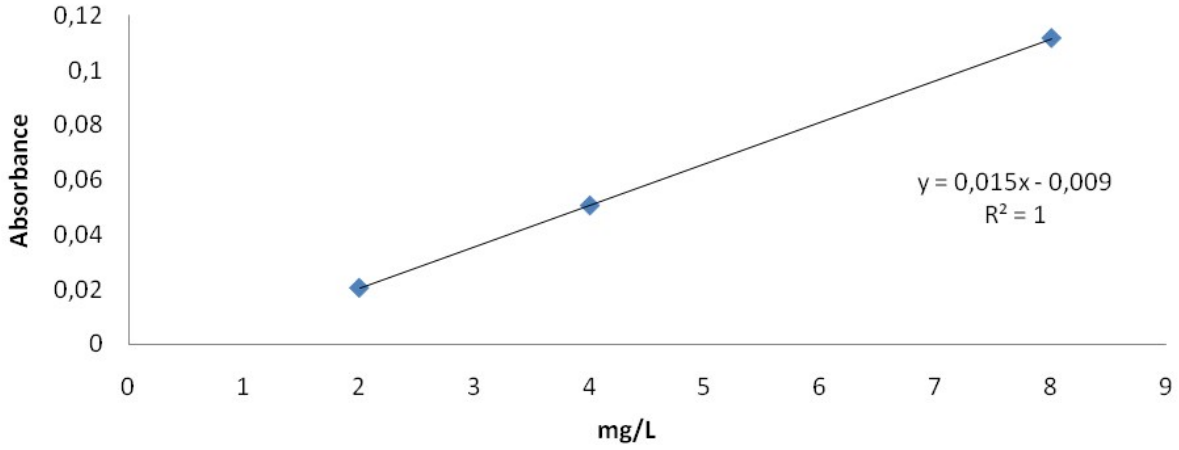

Results :

Sample	**% mass**
	Ru
3a	**0,35**
3b	**0,18**
3c	**0,16**
3d	**0,18**

1.5 Diffuse Reflectance Spectroscopy-UV-Vis

DRS-UV-VIS spectra were recorded on a **UV-Vis-NIR spectrophotometer (Varian-Cary 500)**, and the deconvolution process was recorded in the Fityk 0.9.8. Software (A curve fitting and data analysis program).

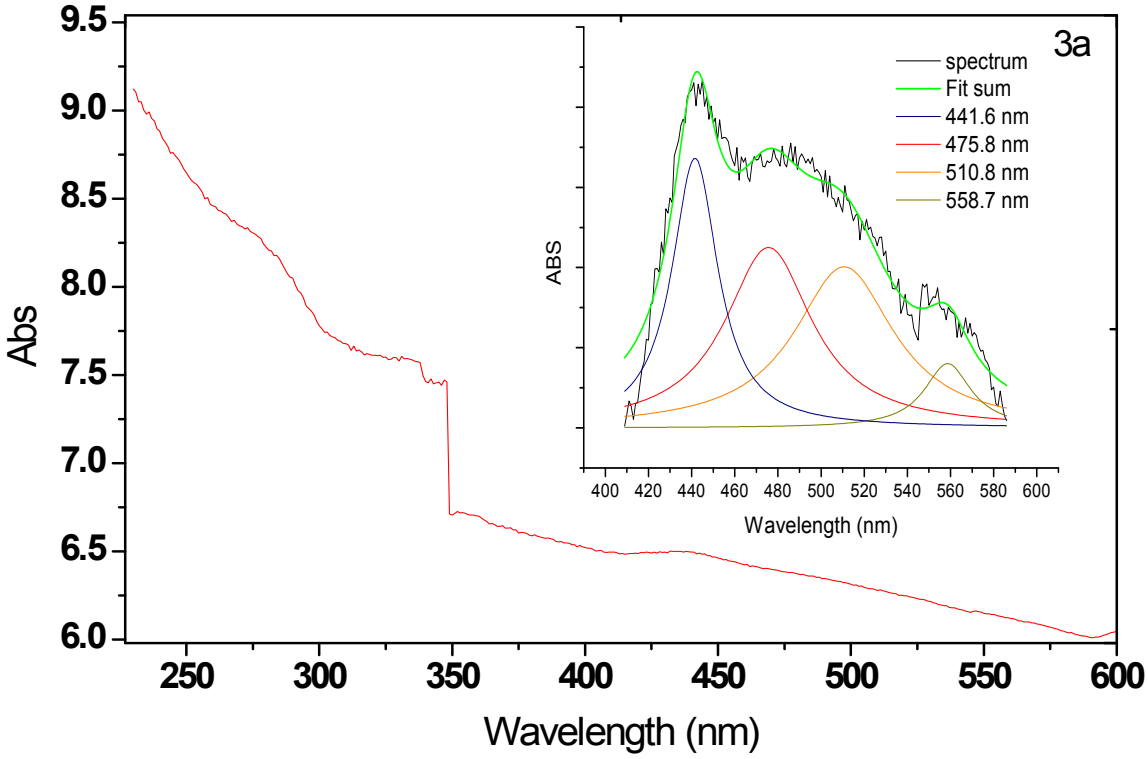

Figure S18. UV-VIS DRS spectra and spectrum deconvolution plot (in the visible region) of **3a** solid.

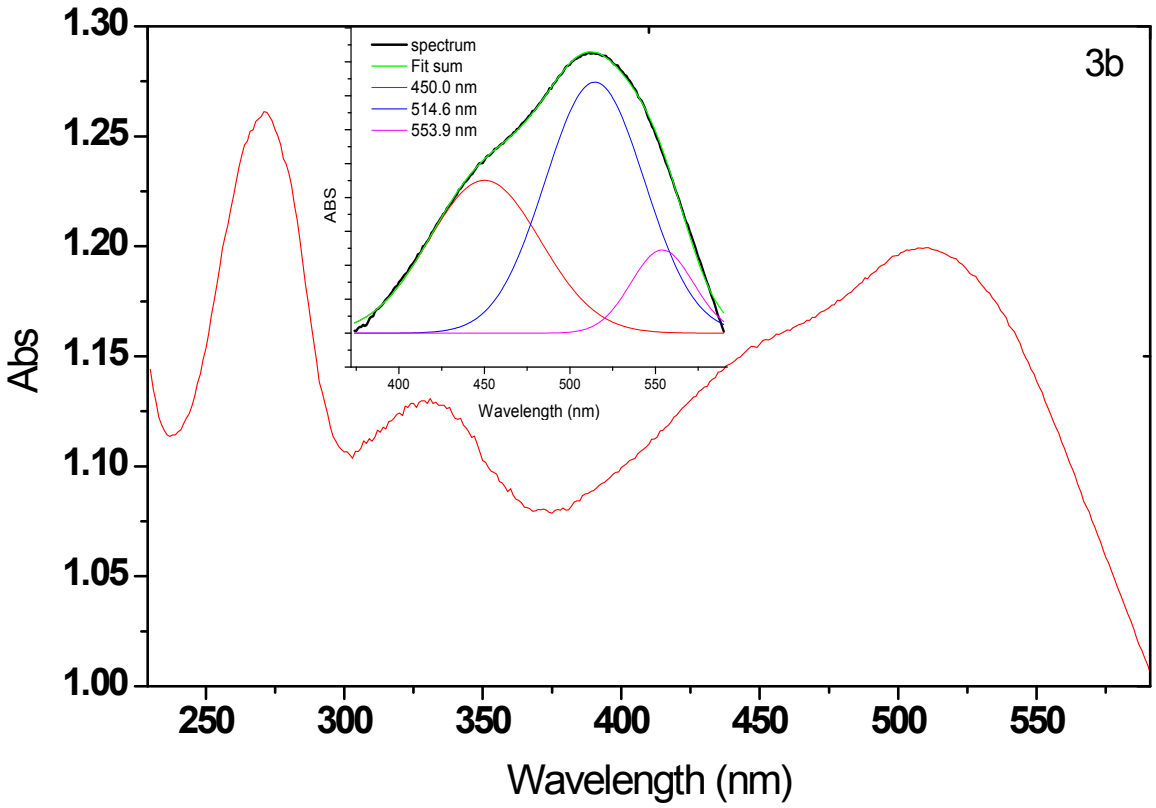

Figure S19. UV-VIS DRS spectra and spectrum deconvolution plot (in the visible region) of **3b** solid.

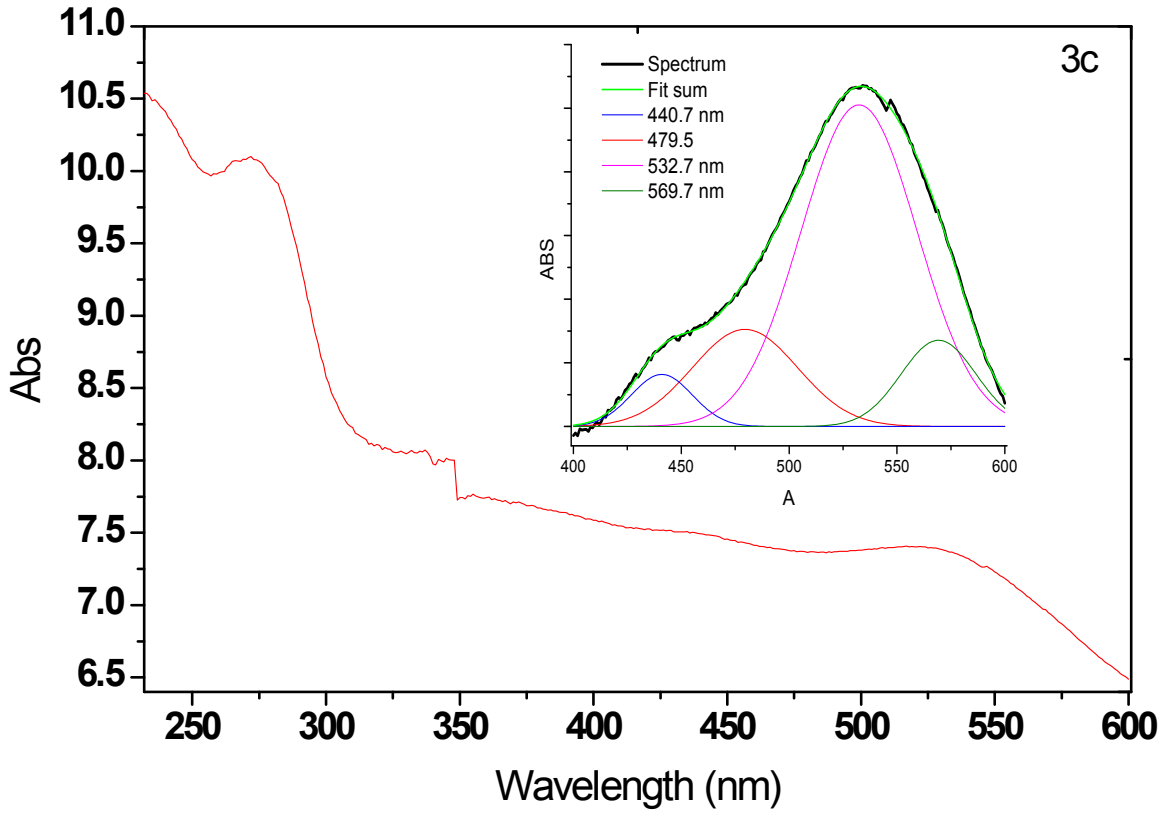

Figure S20. UV-VIS DRS spectra and spectrum deconvolution plot (in the visible region) of **3c** solid.

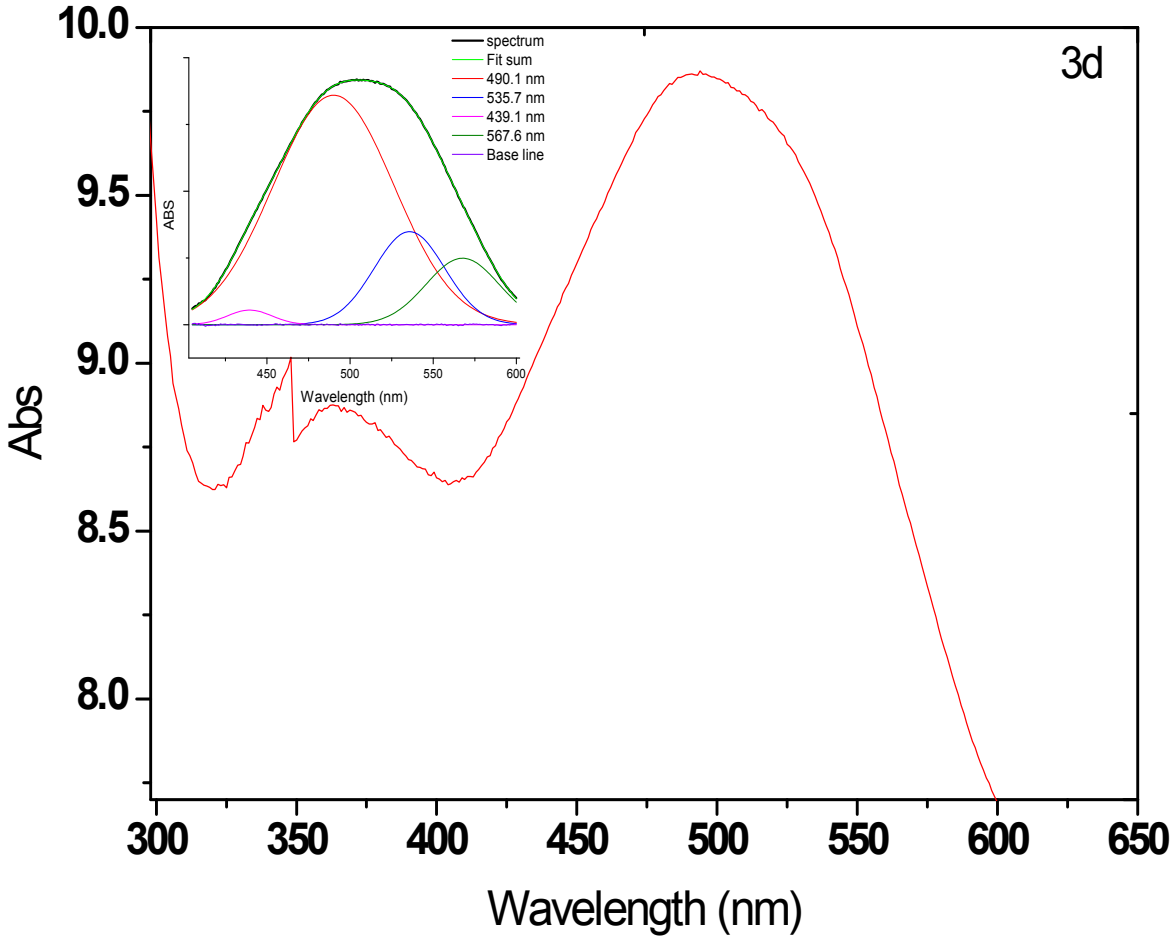

Figure S21. UV-VIS DRS spectra and spectrum deconvolution plot (in the visible region) of **3d** solid.

2. Thermogravimetric analysis (TGA)

Thermogravimetric analyzes (TGA) were performed using **SDT Q600** instrument.

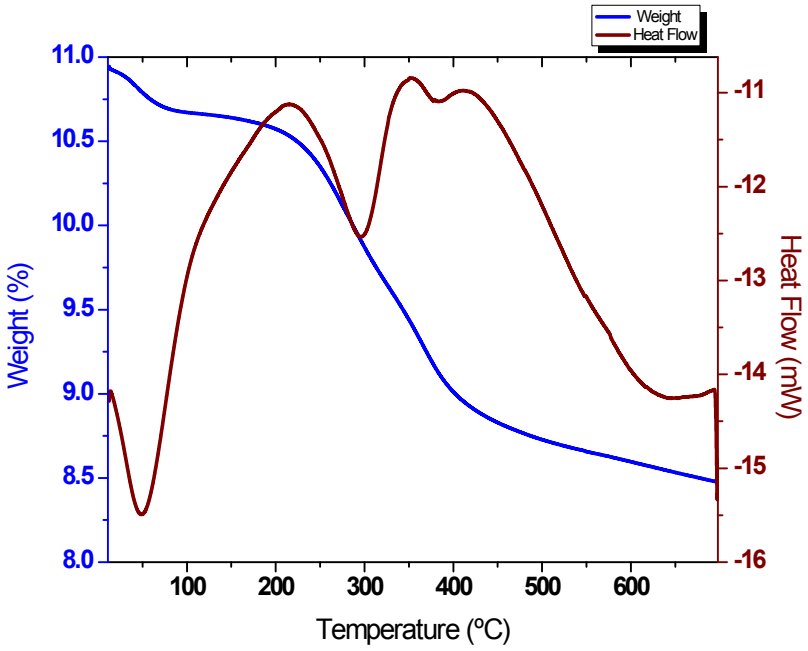

Figure S22. Thermogravimetric analysis (TGA) plot of **3a** solid.

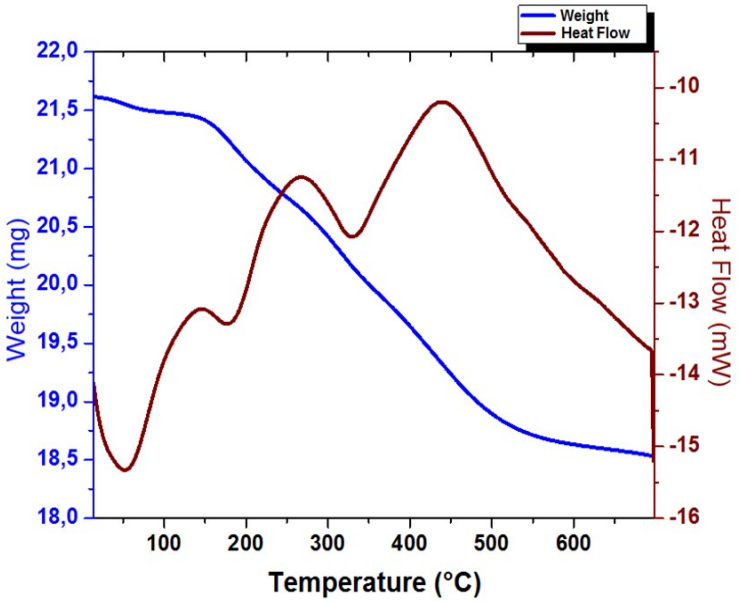

Figure S23. TGA plot of **3b** solid.

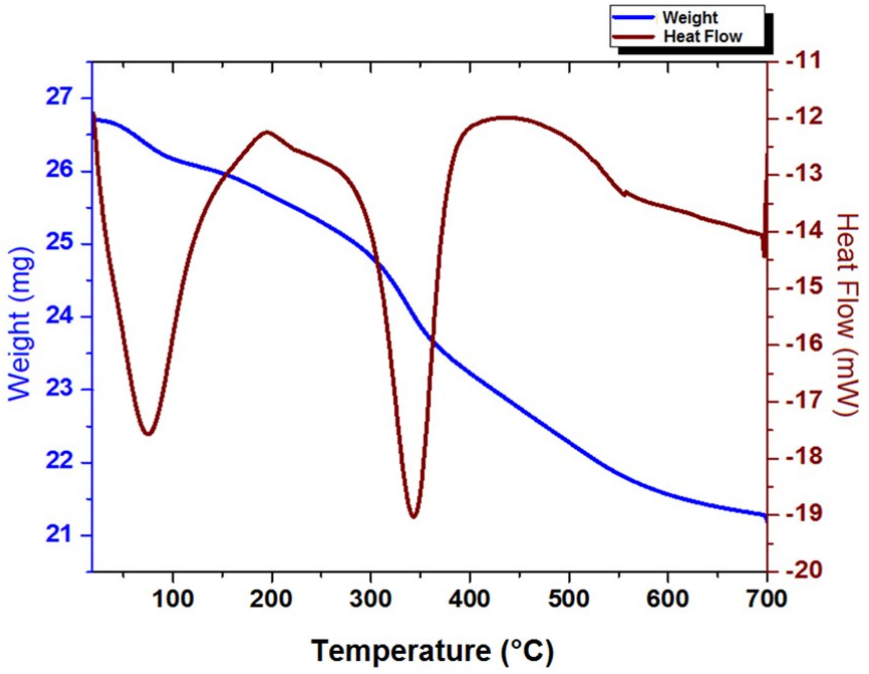

Figure S24. TGA plot of **3c** solid.

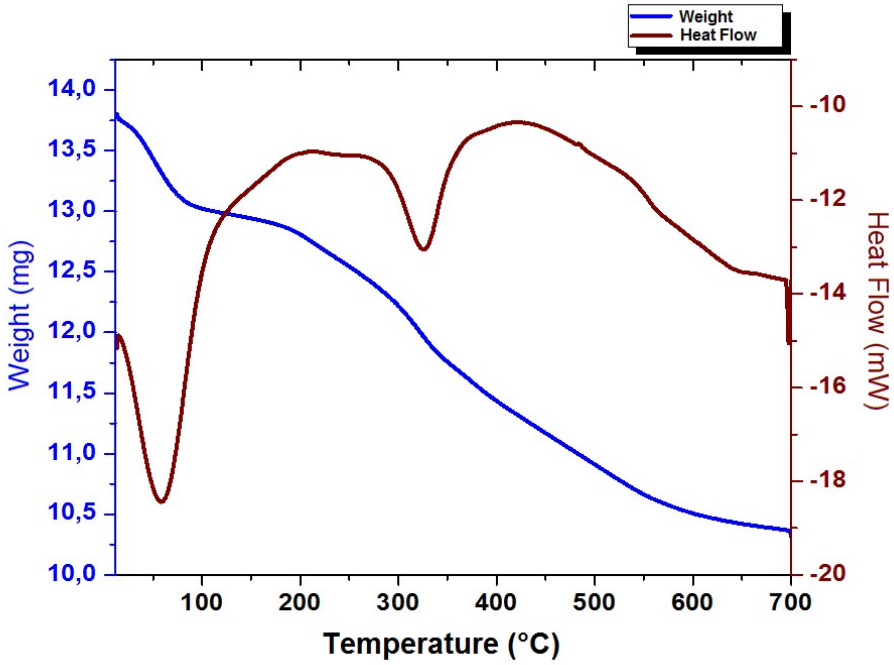

Figure S25. TGA plot of **3d** solid.

3. Braunuer-Emmett-Teller (BET) and Barret-Joyner-Helenda (BHJ) analyses

Braunuer-Emmett-Teller (BET) and Barret-Joyner-Halenda (BHJ) analyses were obtained on TRISTAR 3000 instrument.

3.1 BET and BHJ analysis of 3a solid

Analysis Adsorptive: N2 Analysis Bath Temp.: -195.800 °C

Warm Free Space: 17.6015 cm^3 Measured Cold Free Space: 53.5640 cm^3 Measured

Equilibration Interval: 10 s Low Pressure Dose: None

Automatic Degas: No

Sample Density: 1.000 g/cm^3 Sample Mass: 0.0405 g

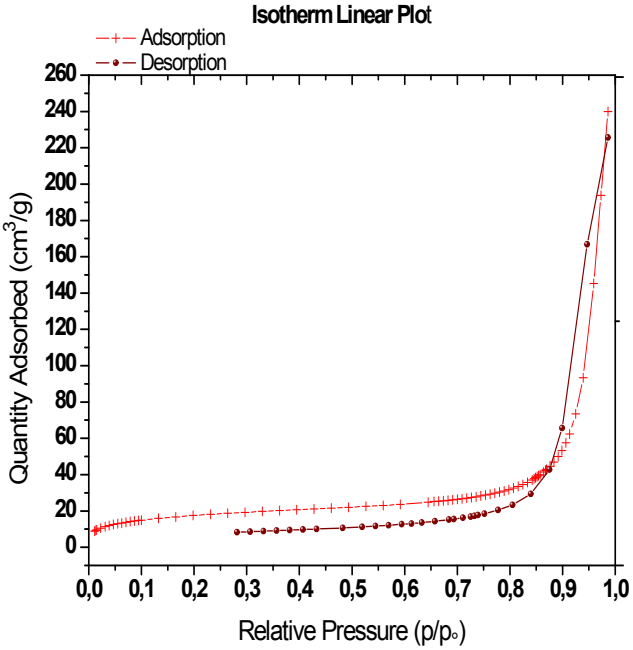

Figure S26. Isotherm Linear Plot of **3a** solid.

BET Surface Area Report

BET Surface Area: 63.0959 ± 0.2984 m^2/g

Slope: 0.068352 ± 0.000325 g/cm^3 STP

Y-Intercept: 0.000641 ± 0.000033 g/cm^3 STP

C: 107.593620

Qm: 14.4942 cm^3/g STP

Correlation Coefficient: 0.9998197

Molecular Cross-Sectional Area: 0.1620 nm^2

t-Plot Report

Micropore Volume: 0.003295 cm^3/g STP

Micropore Area: 9.2572 m^2/g

External Surface Area: 53.8387 m^2/g

Slope: 3.480652 ± 0.113263 $cm^3/g \cdot Å$ STP

Y-Intercept: 2.130409 ± 0.469669 cm^3/g STP

Correlation Coefficient: 0.995791

Surface Area Correction Factor: 1.000

Density Conversion Factor: 0.0015468

Total Surface Area (BET): 63.0959 m^2/g

Thickness Range: 3.5000 Å to 5.0000 Å

Thickness Equation: Harkins and Jura

$$t = [\ 13.99 / (\ 0.034 - \log(p/p^\circ)\ )\ ]\ ^\wedge\ 0.5$$

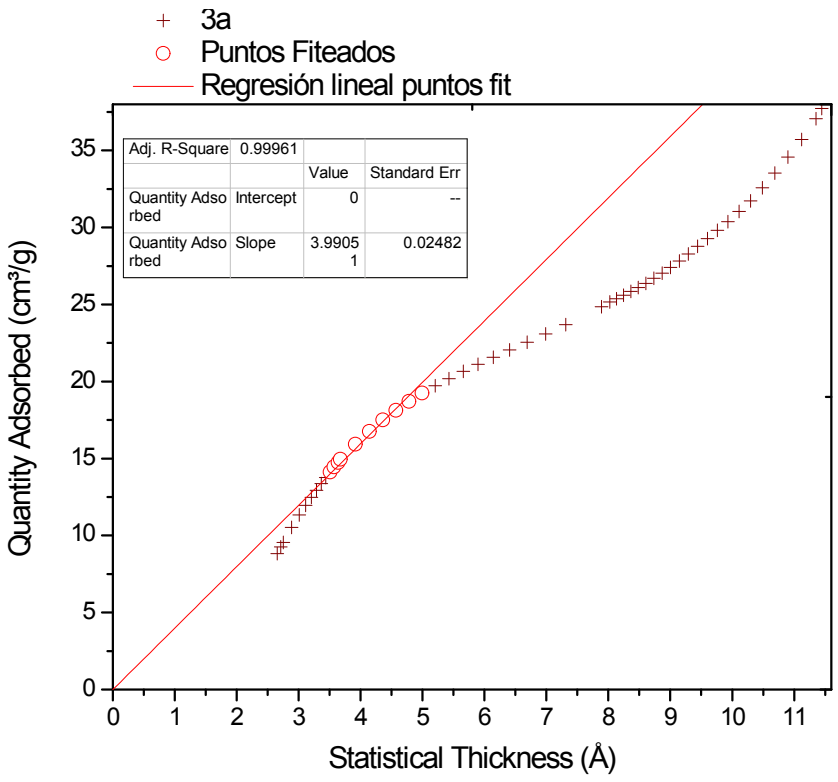

Figure S27. t-Plot Harkins and Jura of **3a** solid.

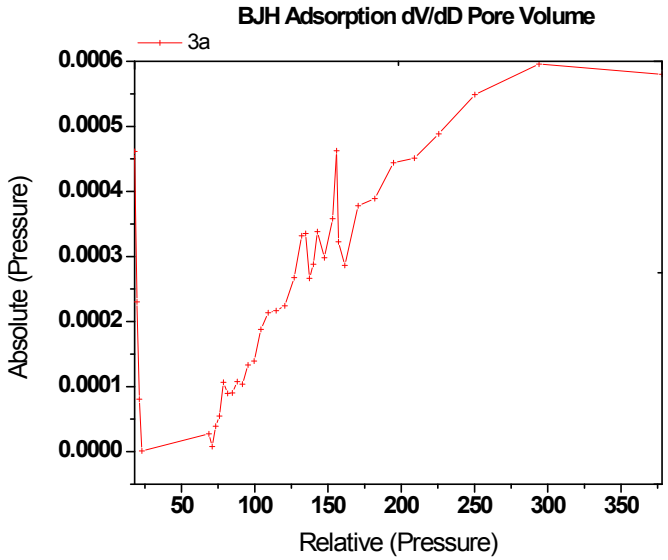

Figure S28. BHJ Adsorption dV/dD pore volume of **3a** solid.

BJH Adsorption Pore Distribution Report

t = [13.99 / (0.034 - log(p/p°))] ^ 0.5

Diameter Range: 17.000 Å to 500.000 Å

Adsorbate Property Factor: 9.53000 Å

Density Conversion Factor: 0.0015468

Fraction of Pores Open at Both Ends: 0.00

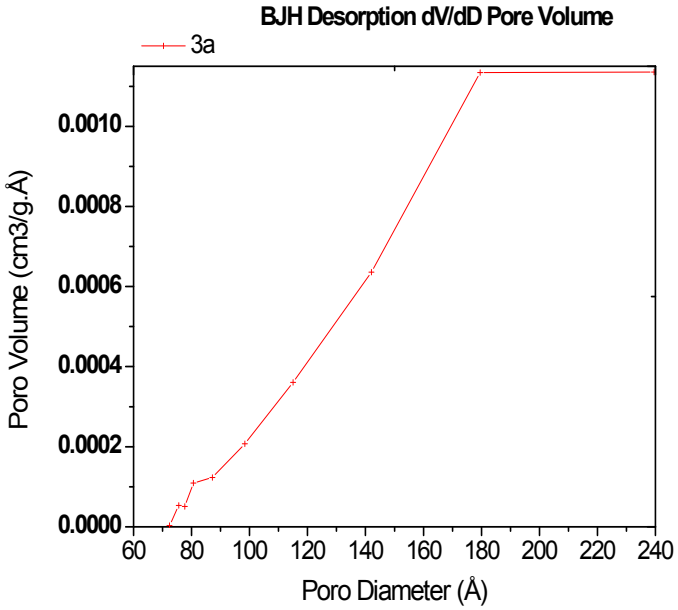

Figure S29. BHJ Desorption dV/dD pore volume of **3a** solid.

BJH Desorption Pore Distribution Report

t = [13.99 / (0.034 - log(p/p°))] ^ 0.5

Diameter Range: 17.000 Å to 500.000 Å

Adsorbate Property Factor: 9.53000 Å

Density Conversion Factor: 0.0015468

Fraction of Pores Open at Both Ends: 0.00

Summary Report

Surface Area

Single point surface area at p/p° = 0.231268014: 60.6967 m^2/g

BET Surface Area: 63.0959 m^2/g

t-Plot External Surface Area: 53.8387 m^2/g

BJH Adsorption cumulative surface area of pores

between 17.000 Å and 500.000 Å diameter: 33.1219 m^2/g

BJH Desorption cumulative surface area of pores

between 17.000 Å and 500.000 Å diameter: 53.7528 m^2/g

Pore Volume

Single point adsorption total pore volume of pores

less than 491.280 Å diameter at p/p° = 0.959281185: 0.224808 cm^3/g

t-Plot micropore volume: 0.003295 cm^3/g

BJH Adsorption cumulative volume of pores

between 17.000 Å and 500.000 Å diameter: 0.198884 cm^3/g

BJH Desorption cumulative volume of pores

between 17.000 Å and 500.000 Å diameter: 0.275397 cm^3/g

Pore Size

BJH Adsorption average pore diameter (4V/A): 240.185 Å

BJH Desorption average pore diameter (4V/A): 204.936 Å

3.2 BET and BHJ analysis of 3b solid.

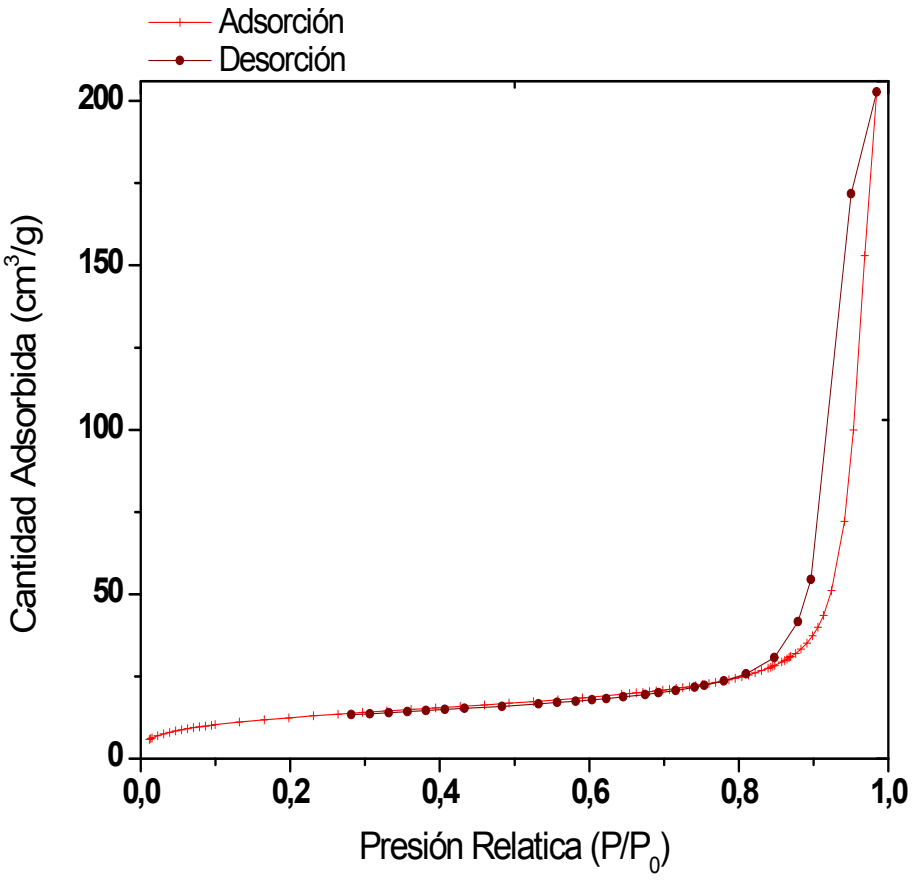

Figure S30. Isotherm Linear Plot of **3b** solid.

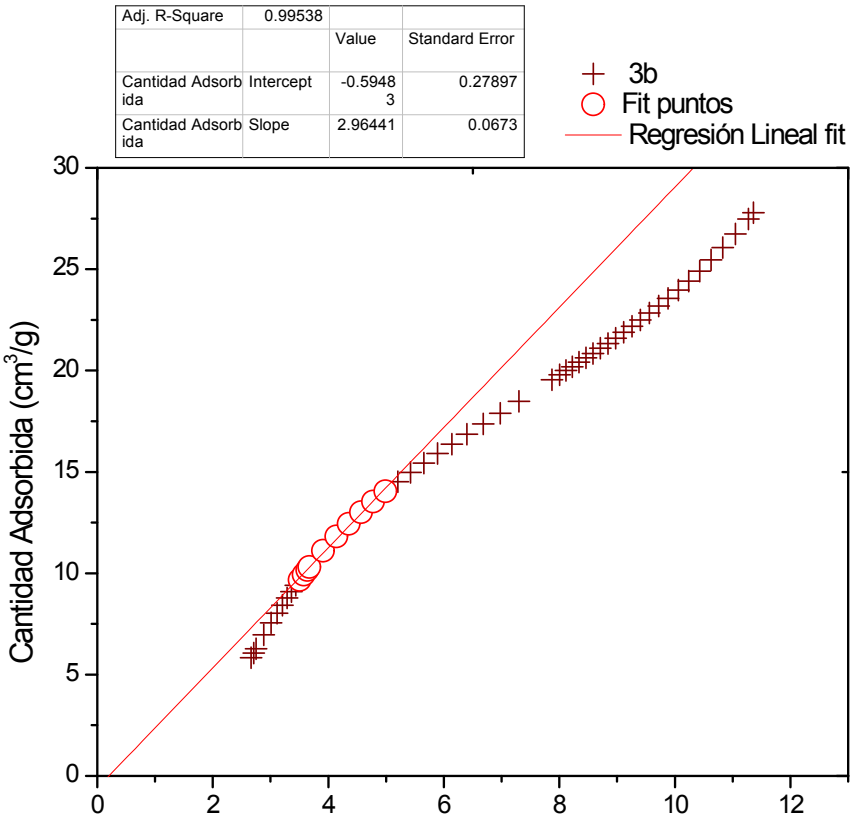

Figure S31. t-Plot Harkins and Jura of **3b** solid.

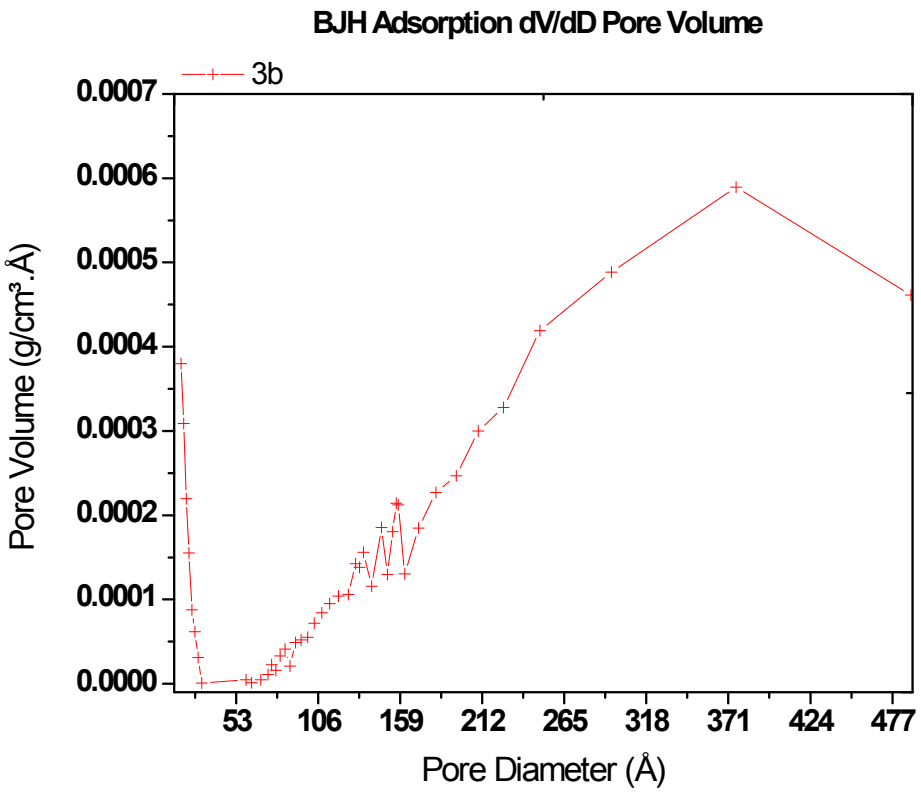

Figure S32. BHJ Adsorption dV/dD pore volume of **3b** solid.

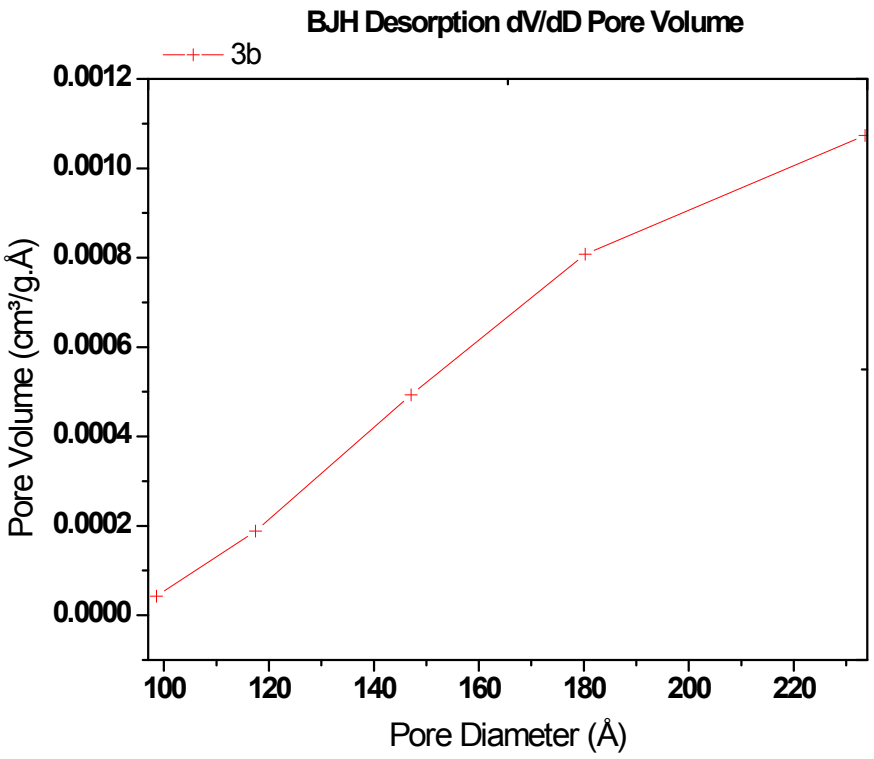

Figure S33. BHJ Desorption dV/dD pore volume of **3b** solid.

Summary Report

Surface Area

Single point surface area at p/p° = 0.230905280: 43.5458 m²/g

BET Surface Area: 45.3262 m²/g

t-Plot External Surface Area: 45.8536 m²/g

BJH Adsorption cumulative surface area of pores

between 17.000 Å and 500.000 Å diameter: 30.8024 m²/g

BJH Desorption cumulative surface area of pores

between 17.000 Å and 500.000 Å diameter: 49.4596 m²/g

Pore Volume

Single point adsorption total pore volume of pores

less than 429.434 Å diameter at p/p° = 0.953180038: 0.154586 cm³/g

t-Plot micropore volume: -0.000920 cm³/g

BJH Adsorption cumulative volume of pores

between 17.000 Å and 500.000 Å diameter: 0.221967 cm³/g

BJH Desorption cumulative volume of pores

between 17.000 Å and 500.000 Å diameter: 0.266242 cm^3/g

Pore Size

BJH Adsorption average pore diameter (4V/A): 288.246 Å

BJH Desorption average pore diameter (4V/A): 215.320 Å

3.3 BET and BHJ analysis of 3c solid.

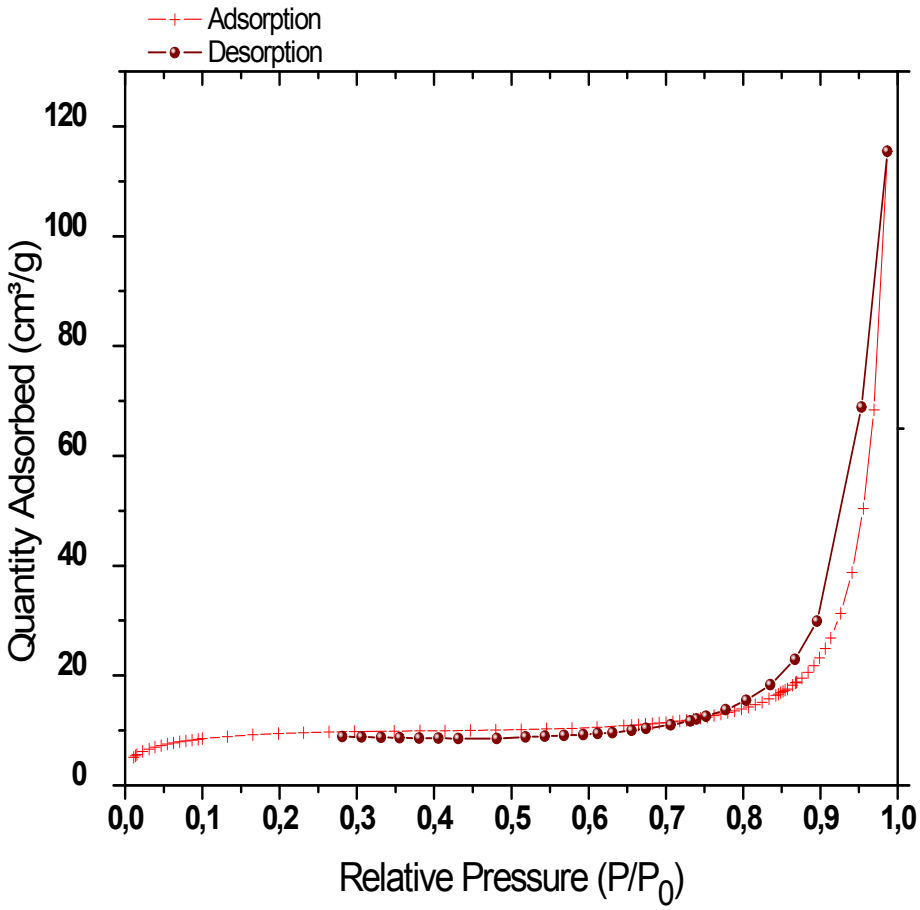

Figure S34. Isotherm Linear Plot of **3c** solid.

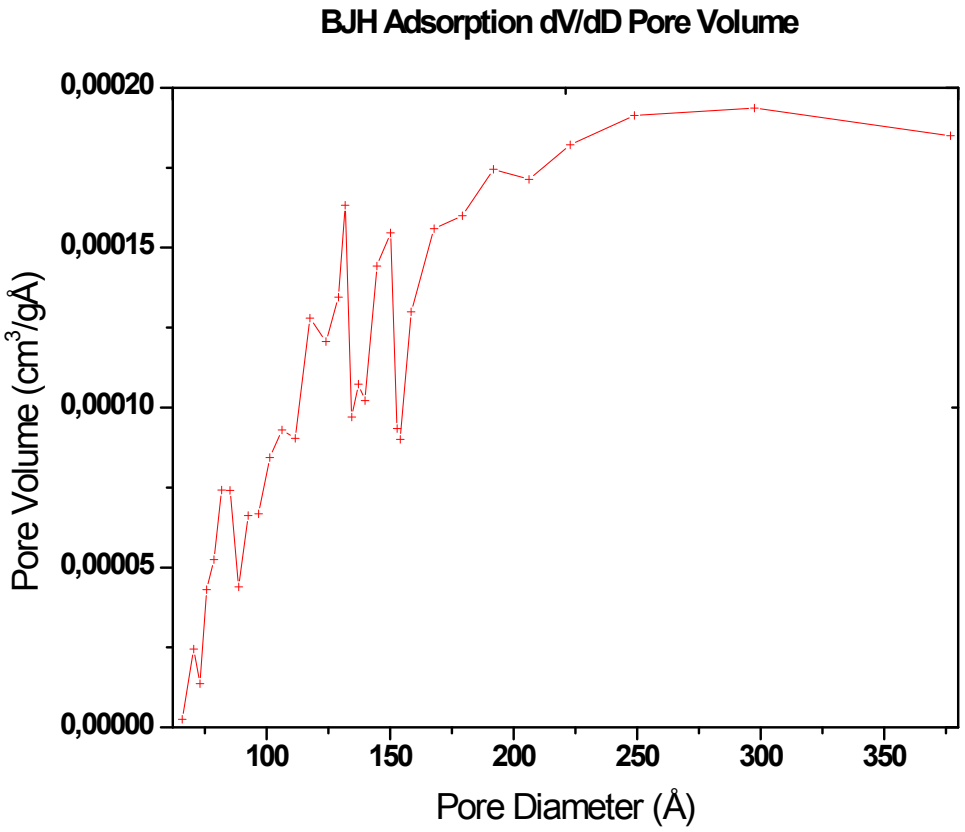

Figure S35. BHJ Adsorption dV/dD pore volume of **3c** solid.

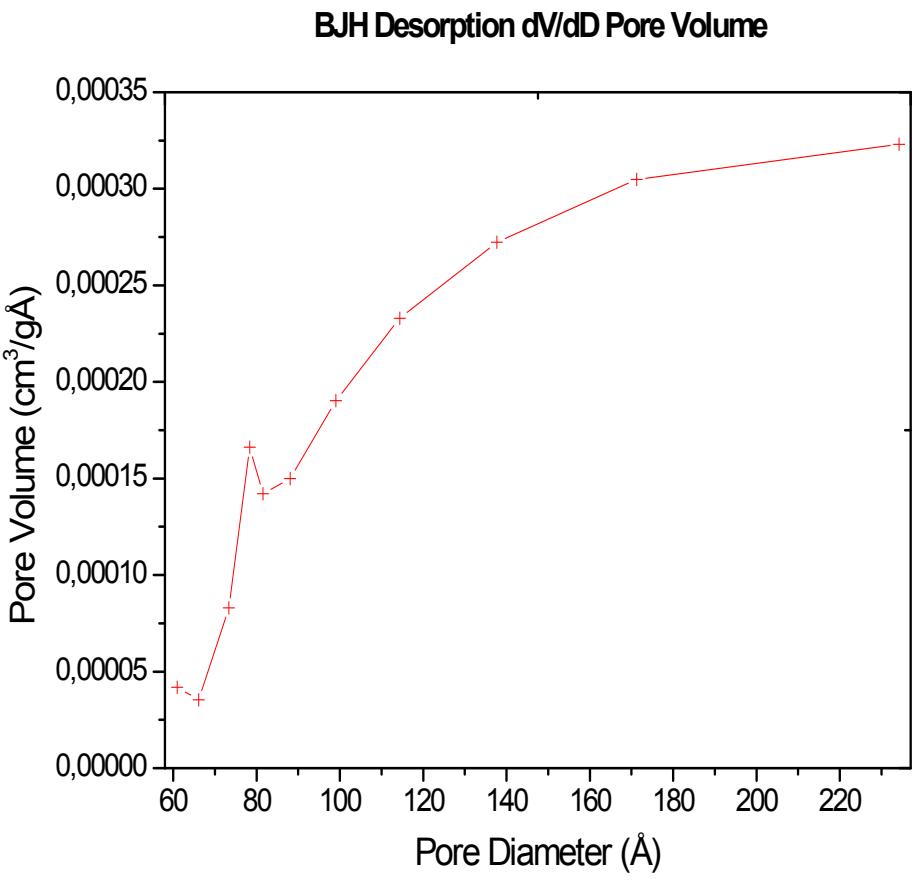

Figure S36. BHJ Desorption dV/dD pore volume of **3c** solid.

Summary Report

Surface Area

Single point surface area at p/p° = 0.231157389: 32.1323 m²/g

BET Surface Area: 33.6192 m²/g

t-Plot External Surface Area: 18.1143 m²/g

BJH Adsorption cumulative surface area of pores

between 17.000 Å and 500.000 Å diameter: 10.5393 m²/g

BJH Desorption cumulative surface area of pores

between 17.000 Å and 500.000 Å diameter: 22.4320 m²/g

Pore Volume

Single point adsorption total pore volume of pores

less than 451.773 Å diameter at p/p° = 0.955581826: 0.077982 cm³/g

t-Plot micropore volume: 0.006456 cm³/g

BJH Adsorption cumulative volume of pores

between 17.000 Å and 500.000 Å diameter: 0.061311 cm^3/g

BJH Desorption cumulative volume of pores

between 17.000 Å and 500.000 Å diameter: 0.106199 cm^3/g

Pore Size

BJH Adsorption average pore diameter (4V/A): 232.696 Å

BJH Desorption average pore diameter (4V/A): 189.371 Å

3.4 BET and BHJ analysis of 3d solid.

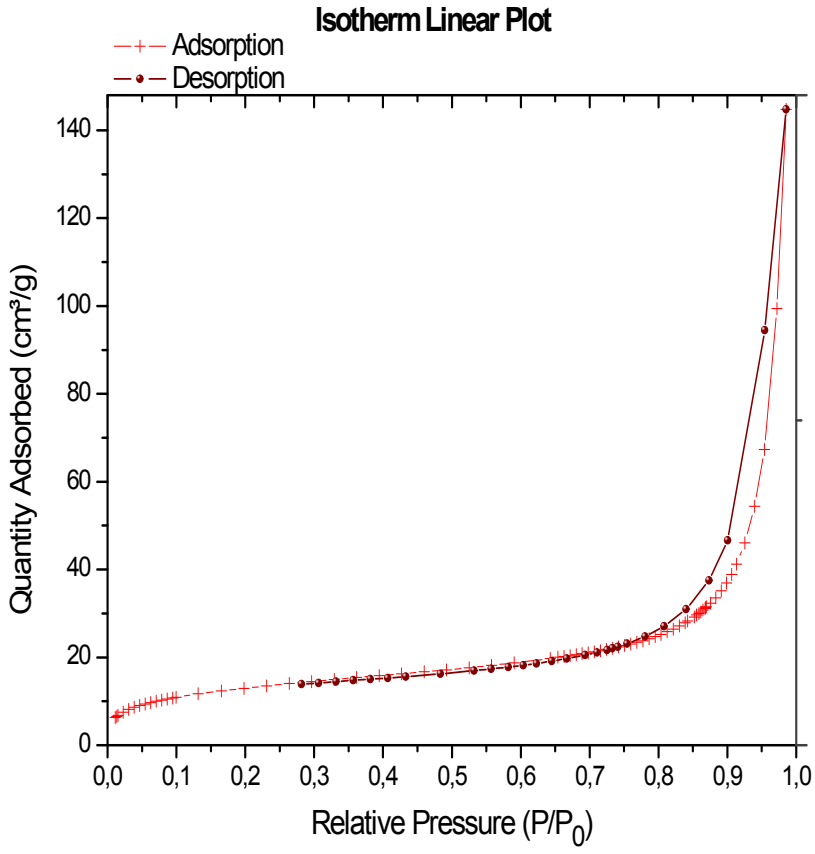

Figure S37. Isotherm Linear Plot of **3d** solid.

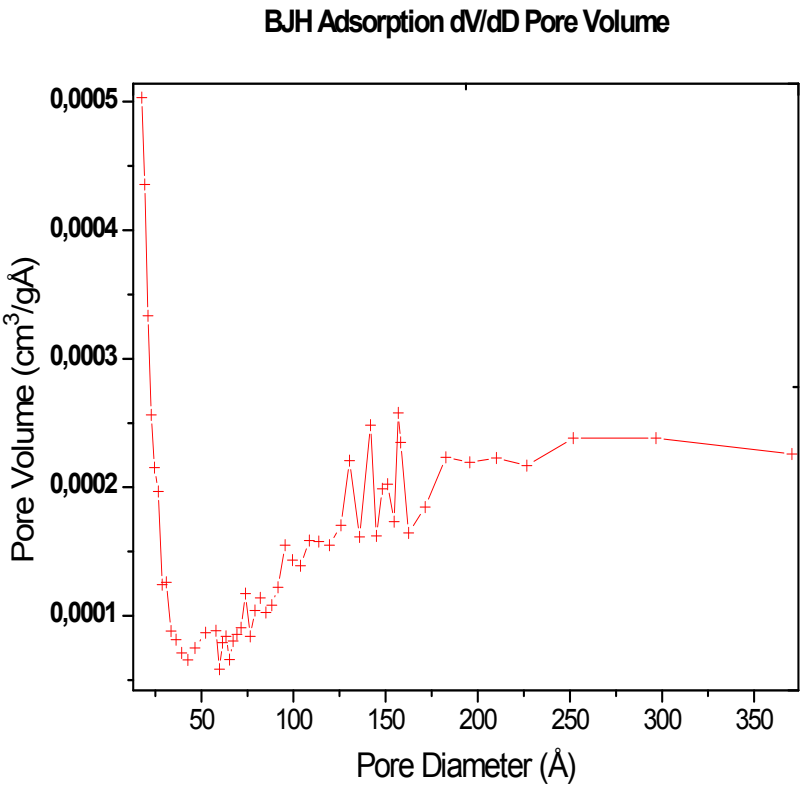

Figure S38. BHJ Adsorption dV/dD pore volume of **3d** solid.

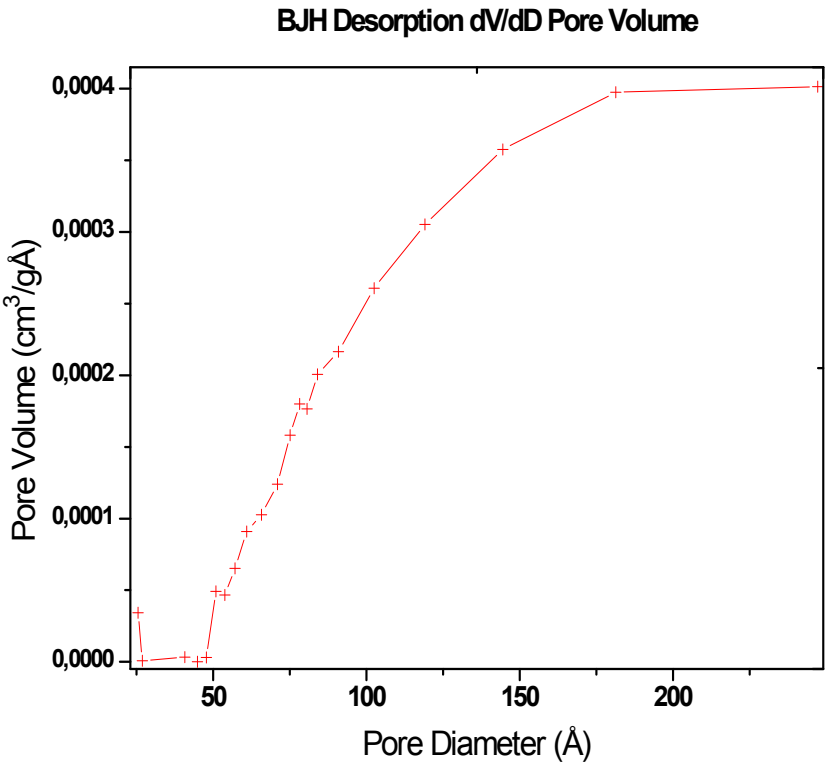

Figure S39. BHJ Desorption dV/dD pore volume of **3d** solid.

Summary Report

Surface Area

Single point surface area at p/p° = 0.230832883: 45.2770 m²/g

BET Surface Area: 47.0552 m²/g

t-Plot External Surface Area: 44.3412 m²/g

BJH Adsorption cumulative surface area of pores

between 17.000 Å and 500.000 Å diameter: 23.6260 m²/g

BJH Desorption cumulative surface area of pores

between 17.000 Å and 500.000 Å diameter: 29.2332 m²/g

Pore Volume

Single point adsorption total pore volume of pores

less than 435.863 Å diameter at p/p° = 0.953897217: 0.104101 cm³/g

t-Plot micropore volume: 0.000563 cm³/g

BJH Adsorption cumulative volume of pores

between 17.000 Å and 500.000 Å diameter: 0.082779 cm³/g

BJH Desorption cumulative volume of pores

between 17.000 Å and 500.000 Å diameter: 0.138529 cm^3/g

Pore Size

BJH Adsorption average pore diameter (4V/A): 140.149 Å

BJH Desorption average pore diameter (4V/A): 189.550 Å

4. Theoretical Data

The ORCA 4.0.1.2 version electronic structure package were used for the geometry optimization, IR spectra and TD-DFT calculations. The functional PBE with resolution of identity approximation (RI), including dispersion correction with Grimme approach (D3) and considering relativistic effects with ZORA were used in all calculations along with the ZORA-Def2-TZVP basis set and SARC/J auxiliary basis set for RI approach.

4.1 Optimized structures

4.1.1 XYZ coordinates

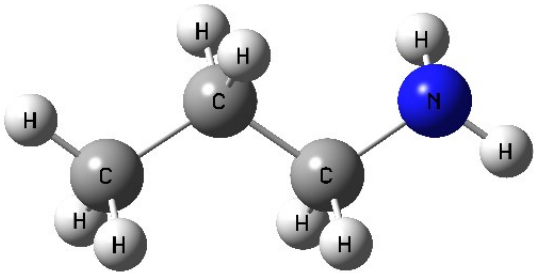

Figure S40. Propylamine optimized geometry.

C	-2.55415210	-0.89153278	-2.84487185
H	-2.59416884	-0.67761229	-3.93484718
H	-2.22872986	-1.94109193	-2.74566706
N	-1.59789178	-0.05615767	-2.10638193
H	-0.65787805	-0.17085240	-2.49070840
H	-1.83735069	0.93102840	-2.22976322
C	-3.95908940	-0.74905305	-2.26508100
H	-4.27158622	0.30800508	-2.33940547
H	-3.91805881	-0.98331797	-1.18929485
C	-4.98386170	-1.63718763	-2.96914009
H	-5.98725593	-1.51264048	-2.53799956
H	-5.05084127	-1.40037985	-4.04230506
H	-4.71413624	-2.70102590	-2.88158958

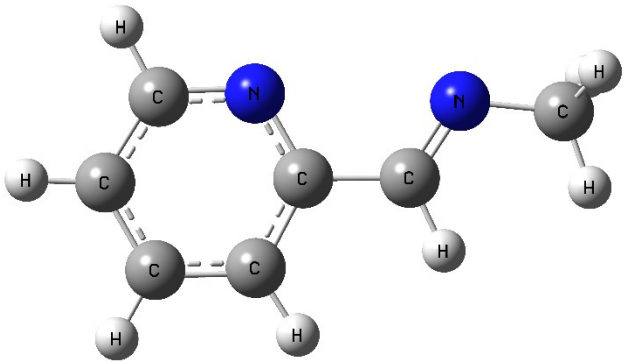

Figure S41. py-CH=N-methyl optimized geometry.

N	-1.75310002	-0.14781258	-2.10110872
C	0.69105493	2.21943279	0.32232688
C	1.50523634	3.22252519	-0.22004949
C	1.48130989	3.41517020	-1.59949357
C	0.65068976	2.60240743	-2.36865398
C	-0.13002886	1.62202345	-1.73358170
N	-0.10955173	1.43250296	-0.39831861
H	2.09765238	4.18384703	-2.06923515
H	0.68665679	2.04251495	1.40321732
H	2.13730572	3.83095262	0.42855677
H	0.60089455	2.71912609	-3.45353826
C	-1.00421885	0.77051460	-2.56815310
C	-2.55517723	-0.90217813	-3.03529768
H	-2.43348929	-0.59529503	-4.09445187
H	-2.30512813	-1.97099516	-2.94053284
H	-3.61626267	-0.80779213	-2.75411825
H	-0.96226263	0.99184491	-3.65732780

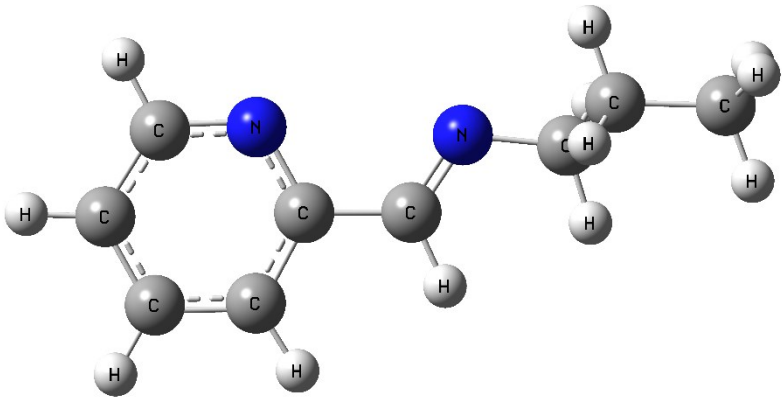

Figure S42. py-CH=N-propyl optimized geometry.

N	-1.72859461	-0.17355145	-2.06988012
C	0.70467099	2.23869282	0.32195460
C	1.50337403	3.24758350	-0.23255556
C	1.46873686	3.42998285	-1.61318838
C	0.64327962	2.60178526	-2.37132848
C	-0.12195153	1.61681903	-1.72454374
N	-0.09086921	1.43707165	-0.38804510
H	2.07294580	4.20259147	-2.09217303
H	0.70920623	2.06943550	1.40408752
H	2.13213504	3.86810024	0.40776958
H	0.58544052	2.70984681	-3.45671660
C	-0.99182965	0.74953652	-2.54732468
C	-2.54212457	-0.93648008	-2.99241154
H	-2.37983692	-0.64027749	-4.05267542
H	-2.24443249	-1.99632804	-2.89625242
H	-0.95798716	0.96211423	-3.63845822
C	-4.02917595	-0.81702493	-2.63886495
H	-4.15740212	-1.08691694	-1.57920374
H	-4.32919805	0.23989088	-2.72910438
C	-4.90852615	-1.69350180	-3.52877191
H	-4.64195039	-2.75697904	-3.42907769
H	-5.97029034	-1.59009889	-3.26395381
H	-4.80262561	-1.42330449	-4.59078797

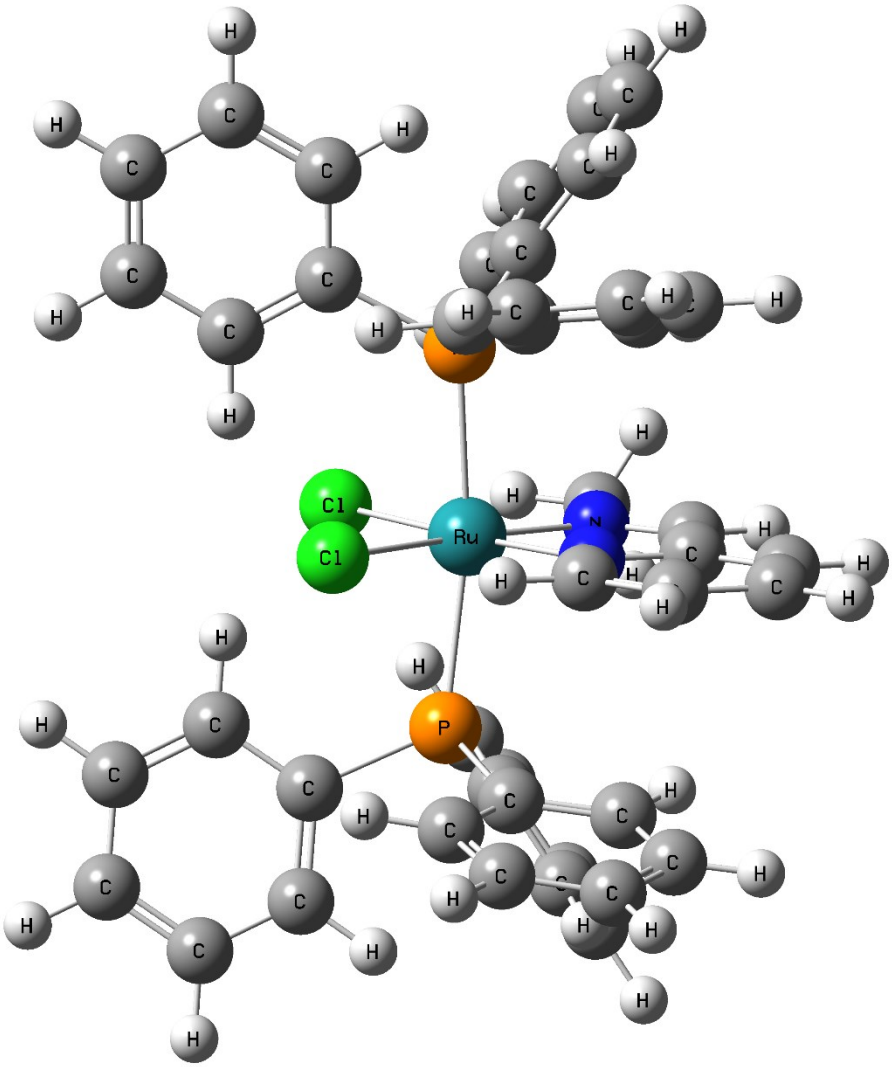

Figure S43. $RuCl_2(PPh_3)_2$(2-Py-CH)=N-CH_3 optimized geometry.

Ru	-1.41220000	-0.46460000	0.14090000
Cl	-0.50020000	1.05140000	1.84150000
Cl	-2.23540000	-2.15250000	1.74140000
N	-2.04570000	-1.48610000	-1.48260000
C	-0.19520000	1.97830000	-1.26290000
C	0.14510000	2.74900000	-2.36690000
C	-0.17600000	2.30260000	-3.65360000
C	-0.83370000	1.08730000	-3.78630000
C	-1.15380000	0.34680000	-2.63920000

N	-0.83410000	0.79370000	-1.37690000
H	0.08300000	2.89450000	-4.53220000
H	0.03000000	2.28150000	-0.23980000
H	0.65990000	3.69610000	-2.20870000
H	-1.10860000	0.69130000	-4.76500000
C	-1.82220000	-0.91720000	-2.64710000
C	-2.71810000	-2.79080000	-1.51690000
H	-2.09020000	-3.51710000	-2.05370000
H	-2.87520000	-3.13950000	-0.49250000
H	-3.68810000	-2.69780000	-2.02680000
H	-2.13080000	-1.39460000	-3.58180000
P	-3.45670000	0.75590000	0.44130000
P	0.75240000	-1.49210000	0.21240000
C	3.52270000	-2.64450000	3.02110000
C	2.84470000	-2.49930000	4.23530000
C	1.52860000	-2.03690000	4.24240000
C	0.88410000	-1.71120000	3.04610000
C	1.56010000	-1.85230000	1.82980000
C	2.88230000	-2.32800000	1.82460000
H	4.55140000	-3.00960000	3.00450000
H	3.34410000	-2.75010000	5.17330000
H	0.99180000	-1.92380000	5.18610000
H	-0.14200000	-1.35170000	3.05150000
H	3.41610000	-2.45160000	0.88020000
C	1.98180000	-0.41870000	-0.62690000
C	2.07120000	-0.38170000	-2.02880000
C	2.92030000	0.52470000	-2.66310000
C	3.67980000	1.42200000	-1.90840000
C	3.57310000	1.41440000	-0.51640000
C	2.72970000	0.50320000	0.12240000
H	1.46550000	-1.05900000	-2.63300000
H	2.97840000	0.53640000	-3.75310000
H	4.34420000	2.13150000	-2.40510000
H	4.14890000	2.12300000	0.08190000

H	2.64020000	0.51360000	1.20880000
C	1.98350000	-3.51430000	-1.44270000
C	2.07720000	-4.82030000	-1.93080000
C	1.13770000	-5.78190000	-1.55560000
C	0.10650000	-5.43240000	-0.67990000
C	0.00330000	-4.12800000	-0.19720000
C	0.93690000	-3.15090000	-0.58210000
H	2.74160000	-2.78460000	-1.72770000
H	2.89640000	-5.08600000	-2.60200000
H	1.21560000	-6.80260000	-1.93490000
H	-0.62410000	-6.18060000	-0.36550000
H	-0.79460000	-3.85870000	0.50000000
C	-5.12830000	1.71510000	4.66850000
C	-3.99560000	0.91030000	4.54500000
C	-3.46620000	0.61790000	3.28510000
C	-4.07660000	1.13220000	2.13670000
C	-5.22250000	1.93550000	2.26350000
C	-5.74250000	2.22930000	3.52240000
H	-5.53640000	1.94170000	5.65550000
H	-3.51190000	0.50330000	5.43480000
H	-2.58300000	-0.00870000	3.18930000
H	-5.71240000	2.33510000	1.37350000
H	-6.63140000	2.85720000	3.60800000
C	-3.45950000	2.61180000	-1.69700000
C	-3.31620000	2.42400000	-0.31180000
C	-2.89570000	3.50660000	0.47690000
C	-2.65880000	4.75420000	-0.10350000
C	-2.83480000	4.93920000	-1.47600000
C	-3.23010000	3.86150000	-2.27200000
H	-3.74260000	1.77400000	-2.33590000
H	-2.74180000	3.36590000	1.54700000
H	-2.33370000	5.58540000	0.52500000
H	-2.65470000	5.91700000	-1.92660000
H	-3.34970000	3.98860000	-3.34960000

C	-5.94690000	0.74040000	-1.02290000
C	-4.99250000	0.02570000	-0.28330000
C	-5.24500000	-1.32030000	0.03030000
C	-6.41640000	-1.93950000	-0.40520000
C	-7.35130000	-1.22880000	-1.16230000
C	-7.11470000	0.11310000	-1.46470000
H	-5.79230000	1.79560000	-1.24910000
H	-4.52200000	-1.87110000	0.63780000
H	-6.59940000	-2.98450000	-0.14700000
H	-8.26630000	-1.71560000	-1.50540000
H	-7.84560000	0.68270000	-2.04210000

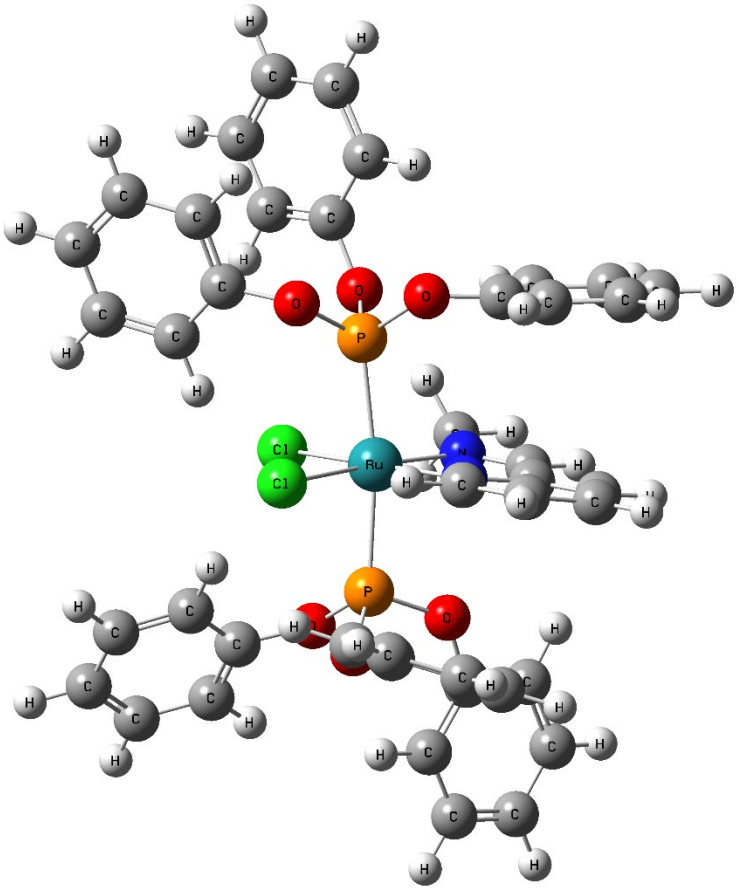

Figure S44. $RuCl_2(P(OPh)_3)_2(2\text{-Py-CH})\text{=N-CH}_3$ optimized geometry.

Ru	-1.26560000	-0.28360000	-0.13140000

Cl	-0.60480000	-0.30610000	2.21800000
Cl	-2.68280000	-2.24850000	0.09360000
N	-1.61790000	-0.08920000	-2.12840000
C	0.60070000	2.13860000	0.25240000
C	1.39740000	3.18640000	-0.19440000
C	1.49420000	3.44870000	-1.56430000
C	0.76710000	2.65880000	-2.44670000
C	-0.02960000	1.62540000	-1.94370000
N	-0.09150000	1.35430000	-0.59800000
H	2.12200000	4.26000000	-1.93410000
H	0.50870000	1.87000000	1.30580000
H	1.95190000	3.77510000	0.53550000
H	0.78740000	2.83870000	-3.52190000
C	-0.89580000	0.80270000	-2.74590000
C	-2.57110000	-0.88790000	-2.88190000
H	-2.58260000	-0.59940000	-3.94440000
H	-2.31200000	-1.94930000	-2.76860000
H	-3.56690000	-0.76500000	-2.43560000
H	-0.98030000	0.96070000	-3.82520000
P	-3.10560000	0.96120000	0.52660000
P	0.47160000	-1.77030000	-0.56500000
C	0.60960000	-6.50570000	1.29910000
C	0.31130000	-6.11930000	2.60800000
C	-0.00500000	-4.78570000	2.87860000
C	-0.02860000	-3.83240000	1.85910000
C	0.27840000	-4.23930000	0.56230000
C	0.59640000	-5.56550000	0.26790000
H	0.85530000	-7.54510000	1.07420000
H	0.32270000	-6.85550000	3.41320000
H	-0.24640000	-4.47390000	3.89650000
H	-0.29390000	-2.79390000	2.06910000
H	0.82500000	-5.84200000	-0.76220000
C	2.65780000	-0.58980000	0.48920000
C	2.81290000	-0.12780000	1.79670000

C	3.66640000	0.94890000	2.03780000
C	4.35440000	1.55930000	0.98460000
C	4.18700000	1.08560000	-0.31820000
C	3.34030000	0.00500000	-0.57490000
H	2.24390000	-0.60410000	2.59380000
H	3.79120000	1.31360000	3.05890000
H	5.02230000	2.40000000	1.18010000
H	4.72130000	1.55450000	-1.14640000
H	3.21810000	-0.38210000	-1.58640000
C	1.60480000	-2.29230000	-4.28420000
C	2.43080000	-3.01750000	-5.14180000
C	3.40910000	-3.86950000	-4.62280000
C	3.55420000	-3.98710000	-3.23940000
C	2.73680000	-3.26520000	-2.36610000
C	1.76060000	-2.41930000	-2.90130000
H	0.82990000	-1.62630000	-4.66690000
H	2.30480000	-2.91790000	-6.22130000
H	4.05410000	-4.43900000	-5.29330000
H	4.31530000	-4.64960000	-2.82340000
H	2.85740000	-3.36080000	-1.28900000
C	-5.77850000	-1.16750000	4.68490000
C	-6.01920000	0.20240000	4.54680000
C	-5.25400000	0.96350000	3.66420000
C	-4.24870000	0.33960000	2.92380000
C	-3.97670000	-1.01890000	3.06070000
C	-4.75930000	-1.76780000	3.94290000
H	-6.38240000	-1.76340000	5.37130000
H	-6.81290000	0.68340000	5.12110000
H	-5.43660000	2.02890000	3.52200000
H	-3.18320000	-1.48180000	2.47540000
H	-4.55970000	-2.83610000	4.04590000
C	-6.55170000	-0.39230000	0.56160000
C	-5.78460000	0.71510000	0.20170000
C	-6.31030000	2.00670000	0.21860000

C	-7.63510000	2.18580000	0.62570000
C	-8.41600000	1.09040000	0.99950000
C	-7.87250000	-0.19730000	0.96230000
H	-6.08700000	-1.37900000	0.54920000
H	-5.68890000	2.85500000	-0.06720000
H	-8.05550000	3.19280000	0.65070000
H	-9.44800000	1.23940000	1.32070000
H	-8.47500000	-1.05670000	1.26030000
C	-3.40530000	2.80370000	-2.12320000
C	-2.82720000	3.23130000	-0.92140000
C	-2.04040000	4.38790000	-0.88820000
C	-1.81620000	5.10550000	-2.06110000
C	-2.36950000	4.67620000	-3.27140000
C	-3.16410000	3.52870000	-3.29270000
H	-4.03900000	1.91820000	-2.13980000
H	-1.60900000	4.70020000	0.06320000
H	-1.19710000	6.00390000	-2.02920000
H	-2.19280000	5.24040000	-4.18820000
H	-3.61540000	3.19230000	-4.22830000
O	-3.05450000	2.60740000	0.28920000
O	-3.51430000	1.17590000	2.07660000
O	-4.47260000	0.46460000	-0.21920000
O	1.87940000	-1.72640000	0.28290000
O	0.26560000	-3.37330000	-0.53000000
O	0.90940000	-1.62730000	-2.13650000

4.2 IR Spectra

IR spectra were calculated at the RI-PBE-D3/Def2-TZVP ZORA level of theory.

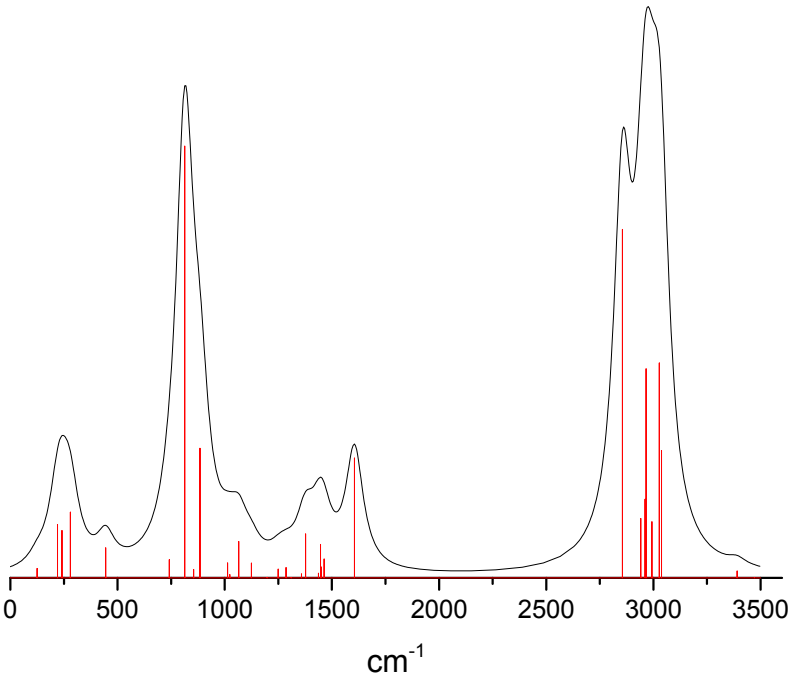

Figure S45. IR spectra of propylamine

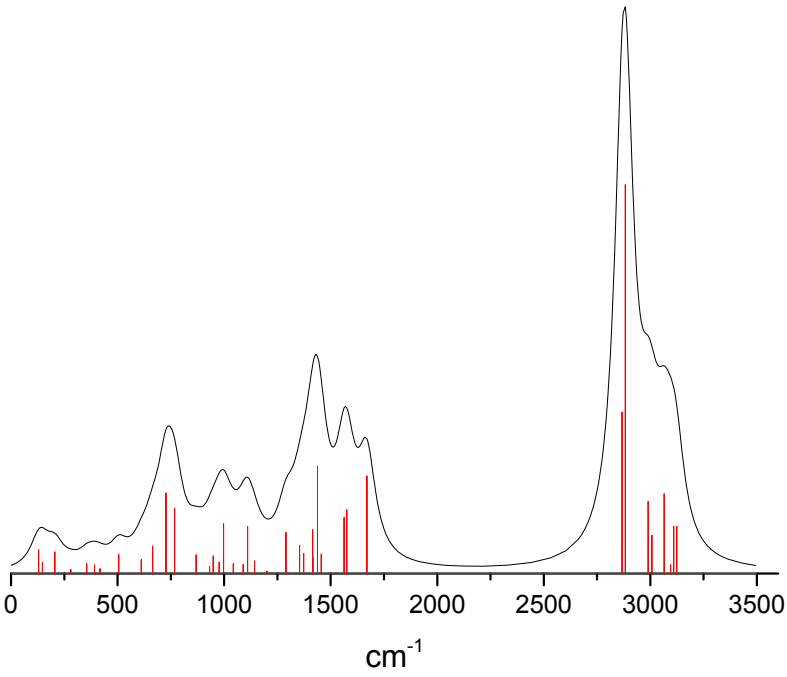

Figure S46. IR spectra of py-CH=N-methyl

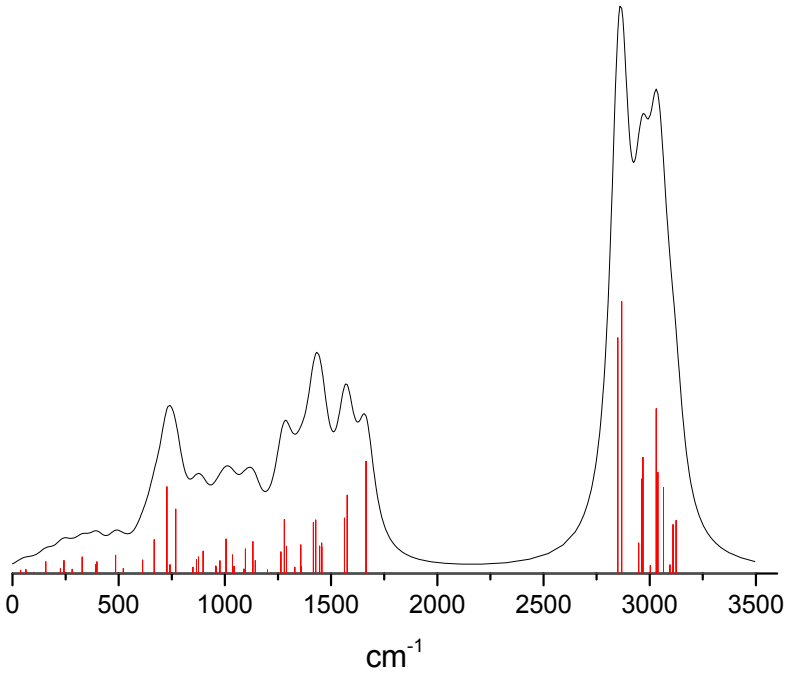

Figure S47. IR spectra of py-CH=N-propyl

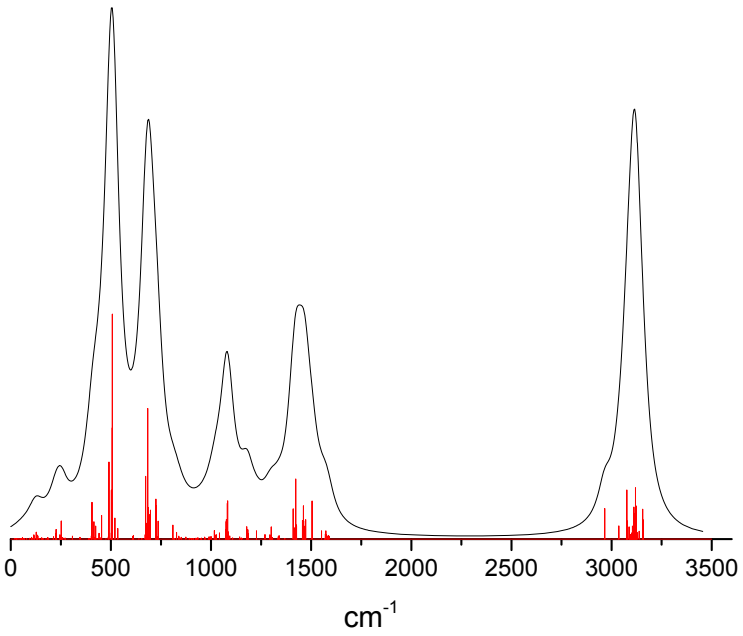

Figure S48. IR spectra of **$RuCl_2(PPh_3)_2$(2-Py-CH)=N-CH_3**

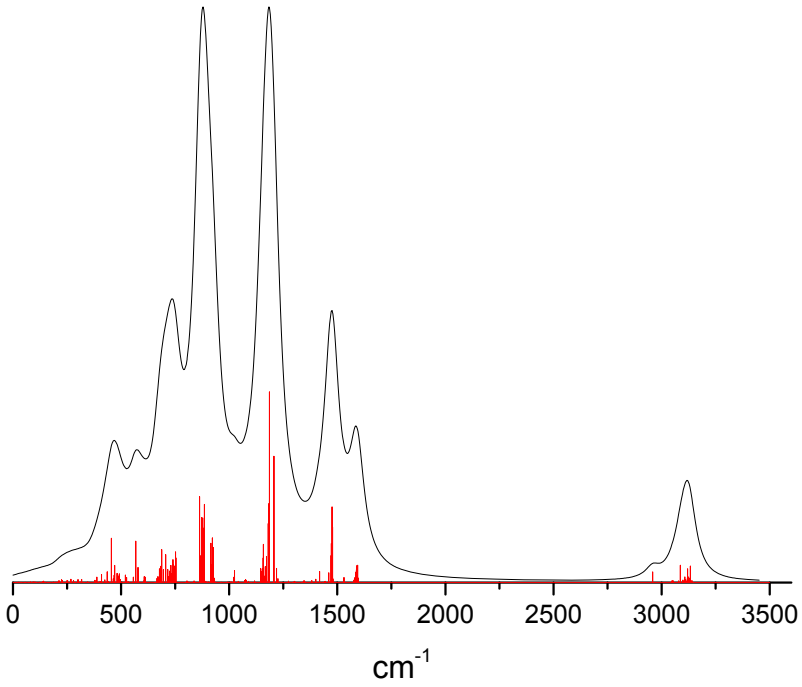

Figure S49. IR spectra of **$RuCl_2(P(OPh)_3)_2$(2-Py-CH)=N-CH_3**

4.3 TD-DFT UV-Vis Spectra

UV-Vis spectra were calculated with TD-DFT approximation at the RI-PBE-D3/ZORA-Def2-TZVP level of theory.

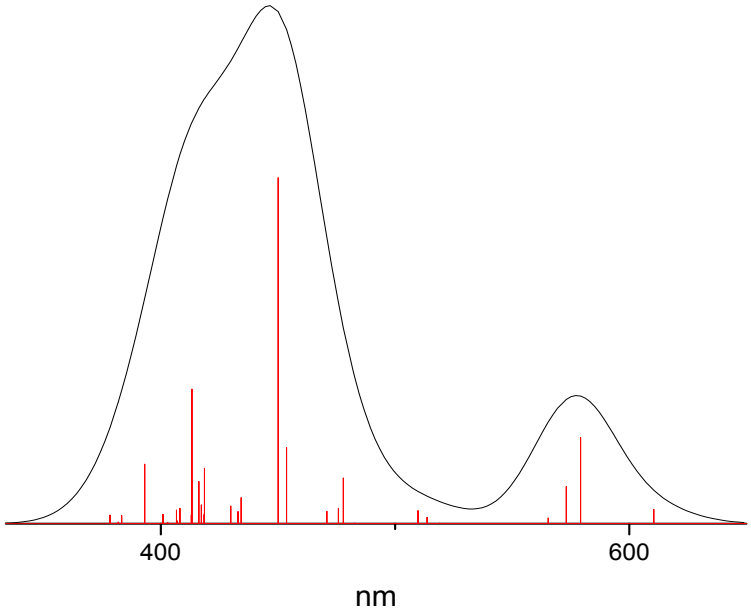

Figure S50. TD-DFT UV-Vis spectra of **$RuCl_2(P(Ph)_3)_2$(2-Py-CH)=N-CH_3**

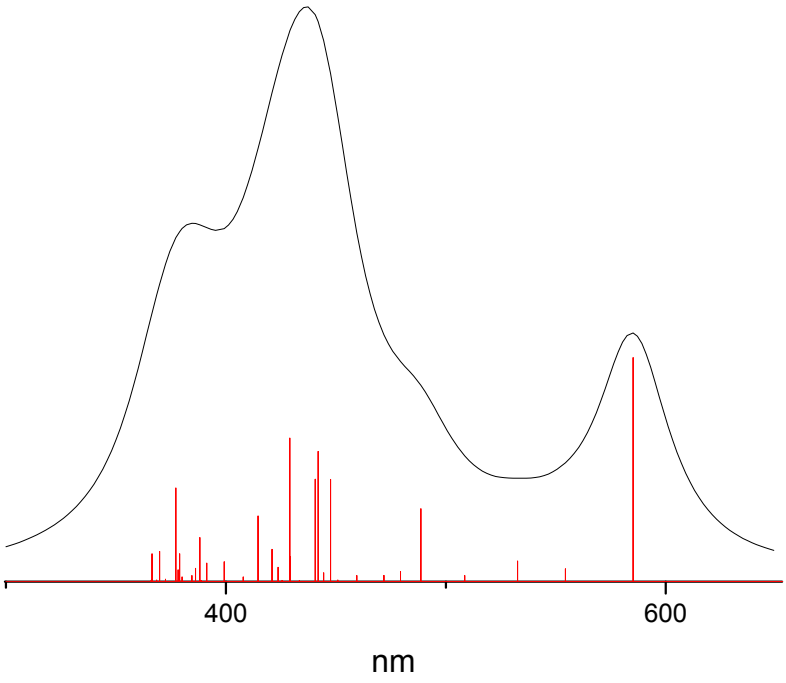

Figure S51. TD-DFT UV-Vis spectra of **$RuCl_2(P(OPh)_3)_2$(2-Py-CH)=N-CH_3**

4.3.1 Natural Transition Orbital

Table S3. $RuCl_2(P(L)_3)_2$(2-Py-CH)=N-CH_3, L=OPh and Ph, UV-Vis spectra Natural Transition Orbitals.

	UV-Vis band wavelength (nm)	State	NTO	NTO population (n)
$RuCl_2(P(Ph)_3)_2$(2-Py-CH)=N-CH_3	579.2	5	HntoS5→LntoS5	0.57199910
			HntoS5-1→LntoS5+1	0.34298016
	573.1	6	HntoS6→LntoS6	0.68830986
			HntoS6-1→LntoS6+1	0.26043363
	509.8	11	HntoS11→LntoS11	0.80031604
			HntoS11-1→LntoS11+1	0.19684552
	477.9	15	HntoS15→LntoS15	0.98349073
	450.1	19	HntoS19→LntoS19	0.59384688
			HntoS19-1→LntoS19+1	0.22284036
			HntoS19-2→LntoS19+2	0.14324326
$RuCl_2(P(OPh)_3)2$(2-Py-CH)=N-	585.1	4	HntoS4→LntoS4	0.92224665

CH_3

554.4	5	HntoS5→LntoS5	0.99570180
532.6	6	HntoS6→LntoS6	0.97077458
488.7	9	HntoS9→LntoS9	0.55428915
		HntoS9-1→LntoS9+1	0.29394483
		HntoS9-2→LntoS9+2	0.15016497

4.3.2 $RuCl_2(P(Ph)_3)_2$(2-Py-CH)=N-CH_3 Natural Transition Orbitals Contour Plots

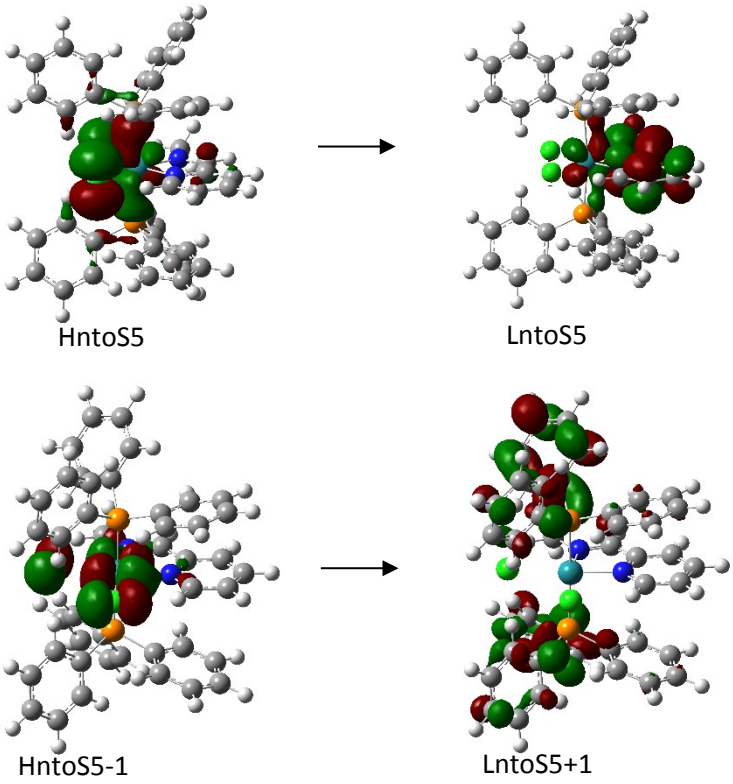

Figure S52. **NTO State 5, λ = 579.2 nm**

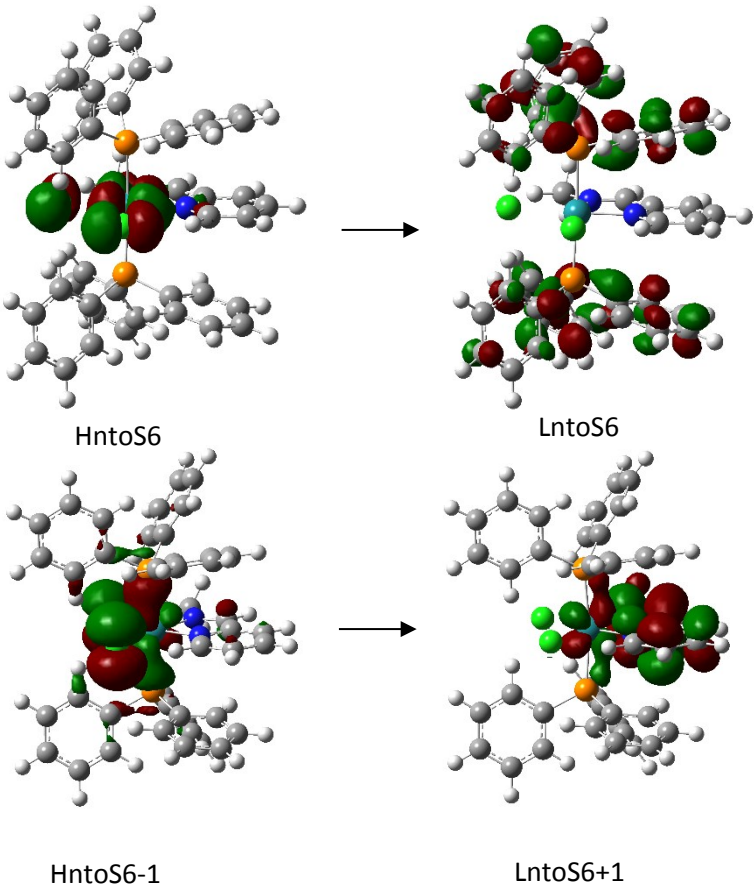

Figure S53. **NTO State 6, λ = 573.1 nm**

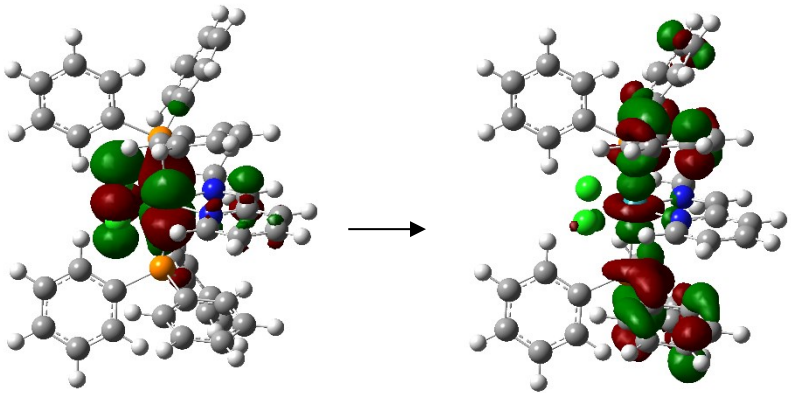

Figure S54. **NTO State 11, λ = 509.8**

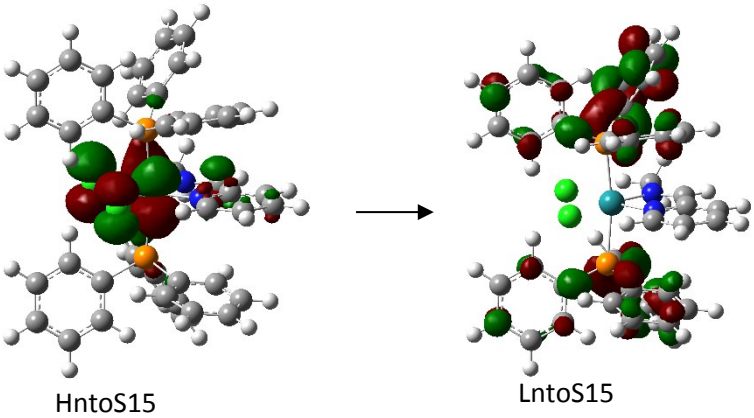

Figure S55. **NTO State 15, λ = 477.9 nm**

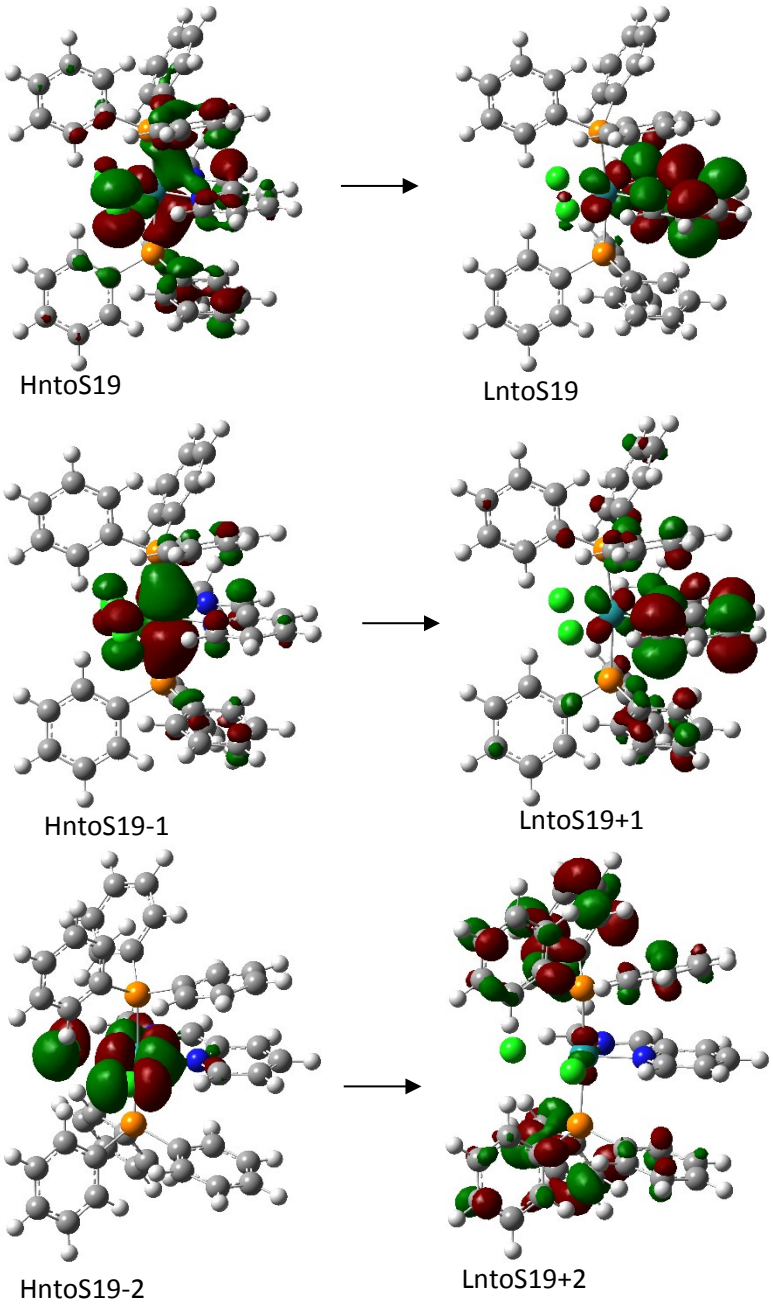

Figure S56. **NTO State 19, λ = 450.1 nm**

4.4.2 $RuCl_2(P(OPh)_3)_2(2\text{-Py-CH})=N\text{-}CH_3$ Natural Transition Orbitals Contour Plots

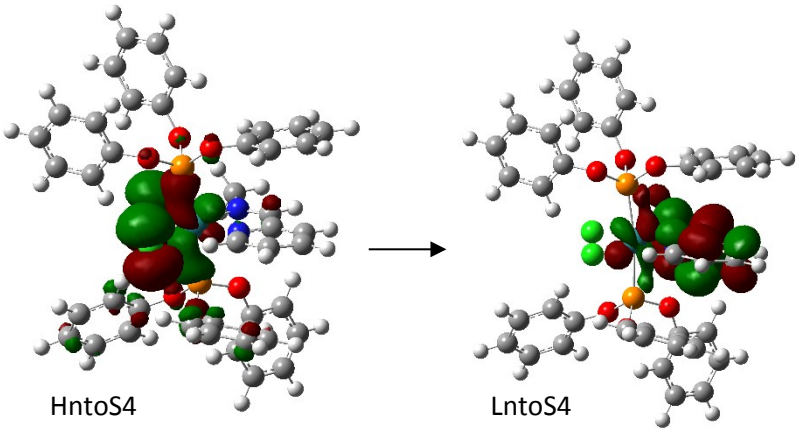

Figure S57. NTO State 4, λ = 585.1 nm

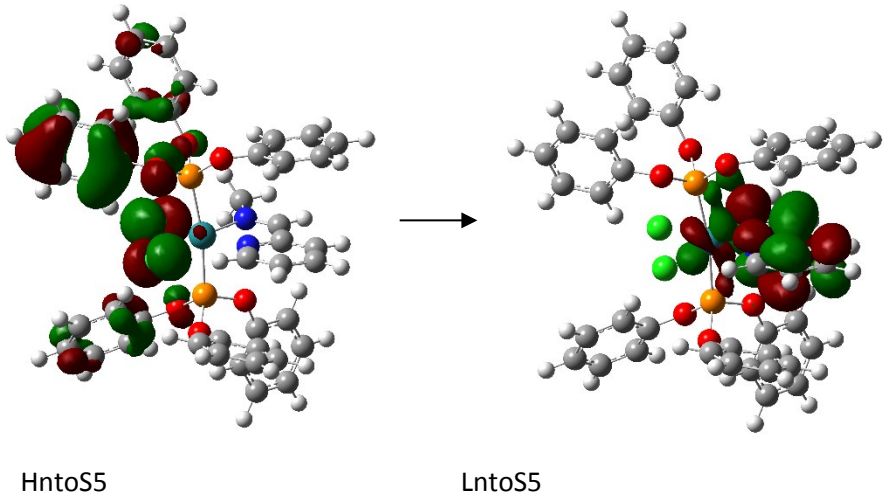

Figure S58. NTO State 5, λ = 554.4 nm

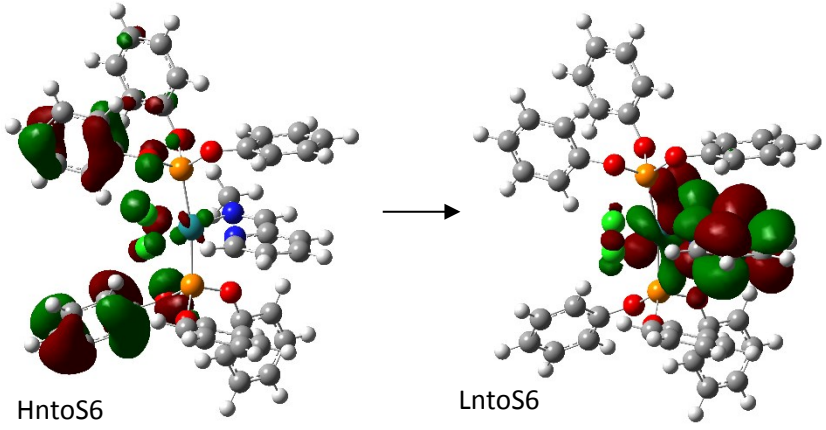

Figure S59. NTO State 6, λ = 532.6 nm

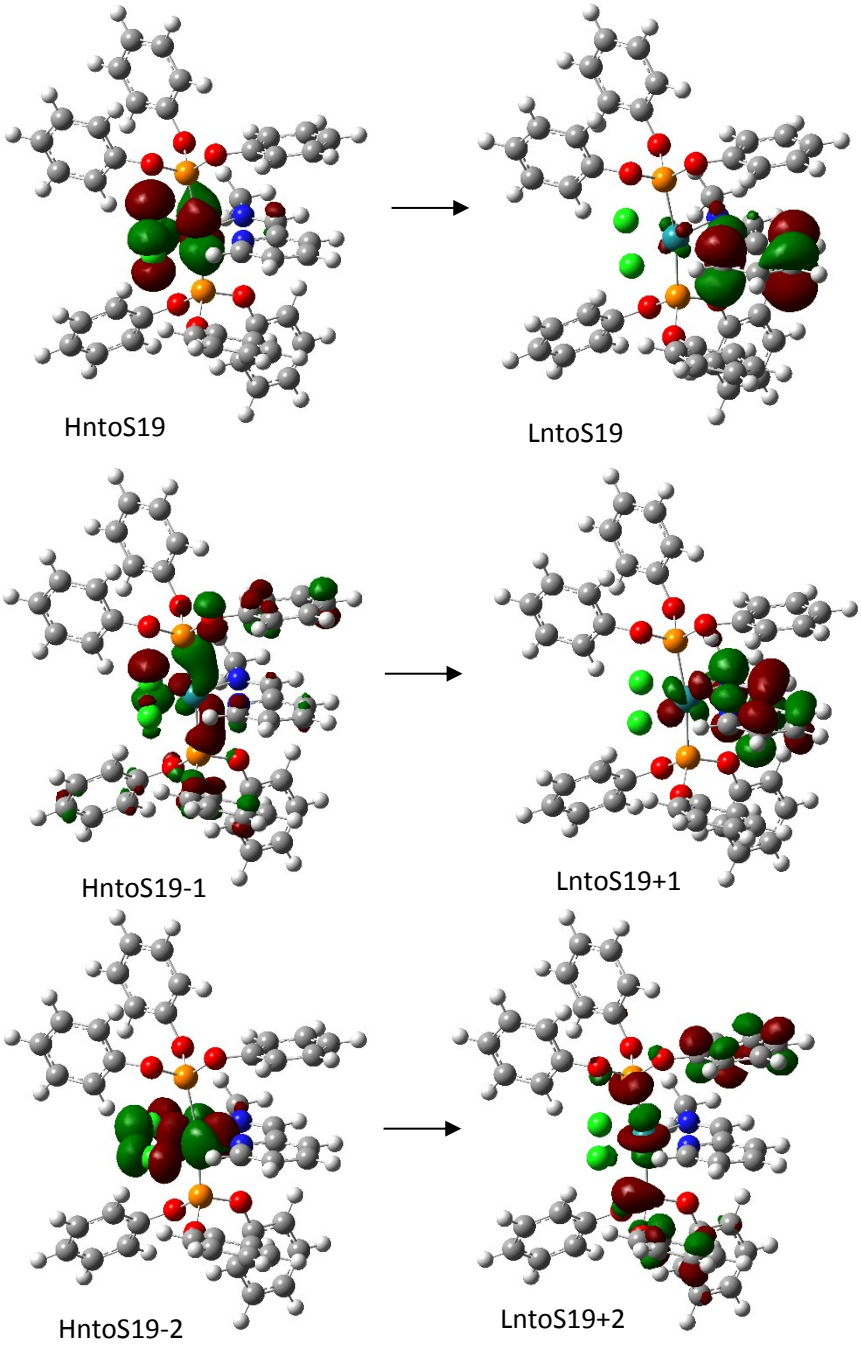

Figure S60. NTO State 9, λ = 488.7 nm